OXFORD

Cerebral Cortex, 2025, **35**, bhaf199
https://doi.org/10.1093/cercor/bhaf199
Advance access publication date 29 July 2025
Original Article

Neurite density but not myelination of specific fiber tracts links polygenic scores to general intelligence

Christina Stammen[1], Javier Schneider Penate[2], Dorothea Metzen[3], Maurice J. Hönscher[4], Christoph Fraenz[1], Caroline Schlüter[4], Onur Güntürkün[4,5], Robert Kumsta[5,6,7], and Erhan Genç[1,*]

[1]Department of Psychology and Neuroscience, Leibniz Research Centre for Working Environment and Human Factors (IfADo), Ardeystraße 67, 44139 Dortmund, Germany
[2]Department of Neuropsychology, Institute of Cognitive Neuroscience, Faculty of Psychology, Ruhr University Bochum, Universitätsstraße 150, 44801 Bochum, Germany
[3]Institute of Psychology, Department of Educational Sciences and Psychology, TU Dortmund University, Emil-Figge-Straße 50, 44227 Dortmund, Germany
[4]Department of Biopsychology, Institute of Cognitive Neuroscience, Faculty of Psychology, Ruhr University Bochum, Universitätsstraße 150, 44801 Bochum, Germany
[5]German Center for Mental Health (DZPG), Partner site Bochum/Marburg, Massenbergstraße 9–13, 44787 Bochum, Germany
[6]Department of Genetic Psychology, Faculty of Psychology, Ruhr University Bochum, Universitätsstraße 150, 44801 Bochum, Germany
[7]Department of Behavioural and Cognitive Sciences, Laboratory for Stress and Gene-Environment Interplay, University of Luxembourg, 2, place de l'Université, 4365 Esch-sur-Alzette, Luxembourg

*Corresponding author: Department of Psychology and Neuroscience, Leibniz Research Centre for Working Environment and Human Factors (IfADo), Ardeystraße 67, 44139 Dortmund, Germany. Email: genc@ifado.de

White matter is fundamental for efficient information transfer and thus crucial for intelligence. Previous studies demonstrated associations between fractional anisotropy and intelligence, but it remains unclear whether this relation is due to greater axon density, parallel, homogenous fiber orientation distributions, or greater myelination, as all influence fractional anisotropy. Using neurite orientation dispersion and density imaging and myelin water fraction imaging, we analyzed the microstructural architecture of intelligence in 500 healthy young adults. We were also interested whether specific white matter indices mediate the pathway linking genetic disposition for intelligence to phenotype. For the first time, we conducted mediation analyses investigating whether neurite density index, orientation dispersion index, and myelin water fraction of 64 white matter tracts mediate the effects of polygenic scores for intelligence on general intelligence (*g*). Our results showed that neurite density index, but not orientation dispersion index or myelin water fraction of white matter tracts, was significantly associated with *g* and that neurite density index of six fiber tracts mediated the relation between genetic variability and *g*. These findings are a crucial step toward decoding the neurogenetic underpinnings of general intelligence, as they identify that neurite density of specific fiber tracts relates polygenic variation to *g*, whereas orientation dispersion and myelination did not.

Keywords: general intelligence; myelin water fraction; neurite density; orientation dispersion; polygenic scores.

Introduction

Intelligence usually refers to the "[. . .] ability to understand complex ideas, to adapt effectively to the environment, to learn from experience, to engage in various forms of reasoning, to overcome obstacles by taking thought" (Neisser et al. 1996). It is one of the most studied human phenotypes, and the last decades have produced cognitive tests in abundance to measure intelligence (Deary et al. 2022). Although the various tests capture different aspects of intelligence, such as reasoning abilities or processing speed (Flanagan and Dixon 2013), individuals who perform well on one test tend to achieve high scores on other cognitive tests, regardless of the skills required (Spearman 1904; Deary et al. 2022). Spearman (1904) concluded that there was a factor of general intelligence, *g*, positioned at the apex of the hierarchy, with broader cognitive domains situated below and more specific cognitive abilities at the base (Schneider and McGrew 2012; Flanagan and Dixon 2013). The *g* factor illustrates the generalist character of intelligence (Plomin and von Stumm 2018), which is also reflected in the numerous associated life outcomes, such as school performance (Roth et al. 2015), job performance (Schmidt and Hunter 2004), socioeconomic success (Strenze 2007), income (Zagorsky 2007), or physical health (Calvin et al. 2017). In addition to the predictive value of intelligence, interindividual differences have been shown to be stable across the lifespan (Deary 2014). Consequently, there have been countless research efforts to uncover the neurogenetic mechanisms from which interindividual differences in intelligence arise.

A well-known framework for understanding intelligence on a neurobiological level provides the Parieto-Frontal Integration Theory of intelligence (P-FIT; Jung and Haier 2007). This model suggests that intelligence is based on numerous areas throughout the cortex, especially in frontal and parietal regions, which are

Received: February 15, 2025. **Revised:** June 7, 2025. **Accepted:** June 30, 2025

strongly interconnected and enable efficient information transfer. The idea that a brain network underlies intelligence also emphasized the role of structural connections, which are present in the form of white matter fiber tracts (Jung and Haier 2007).

One technique to quantify white matter properties is diffusion-weighted imaging, whose advent has ushered in a new era of white matter brain imaging studies (Le Bihan 2003; Deary et al. 2022). As the diffusion of water molecules is a three-dimensional process that includes random translational motion of molecules in space, diffusion anisotropy allows inferences about the presence of obstacles such as axons and their myelin sheaths (Le Bihan 2003). Most studies use fractional anisotropy (FA) as a summative metric to describe white matter microstructural integrity (Genç and Fraenz 2021). In this context, higher FA values suggest more parallel diffusion pathways (Basser and Pierpaoli 1996; Assaf and Pasternak 2008).

The relation between FA and intelligence has been widely studied (Chiang et al. 2009; Penke et al. 2010; Tamnes et al. 2010; Tang et al. 2010; Penke et al. 2012; Booth et al. 2013; Dunst et al. 2014; Kievit et al. 2014; Cremers et al. 2016; Kievit et al. 2016; Malpas et al. 2016; Kievit et al. 2018; Cox et al. 2019; Góngora et al. 2020; Hidese et al. 2020; Holleran et al. 2020; Meinert et al. 2022; Stammen et al. 2023). The majority of studies reported positive associations between average FA values from many major white matter fiber tracts and cognitive performance (Genç and Fraenz 2021). Cox et al. (2019), for example, used a large sample from the UK Biobank study and reported significant positive associations between FA and general intelligence in 25 out of 27 white matter fiber tracts. As summarized by Gençand Fraenz et al. (2021), FA values of the genu and the splenium of the corpus callosum, the uncinate fasciculus, and the superior longitudinal fasciculus were most often associated with differences in intelligence. In one recent study, Stammen et al. (2023) showed robust associations between FA and general intelligence in four independent samples, located around the left-hemispheric forceps minor, superior longitudinal fasciculus, and cingulum-cingulate gyrus.

Since general intelligence appears to be robustly associated with higher FA values and thus stronger anisotropic diffusion patterns, Stammen et al. (2023) formulated three possible explanations as to why higher FA values could be associated with higher intelligence. First, the relation could be due to greater axon density, enabling more parallel information processing by providing more pathways to think through problems relatively simultaneously. Second, the relation could be due to parallel, homogenous fiber orientation distributions that run directly from one brain region to another, thereby enabling more direct and efficient information transfer throughout the brain. Third, the relation could be due to greater myelination, enabling faster information processing speed and signal conduction velocity (Laule et al. 2007; Nave 2010). However, the exact neurobiological basis causing FA signal differences remains unclear, so the hypotheses put forward cannot be tested by looking at FA values alone. FA is a multifaceted and nonspecific metric influenced by various physiological factors, including axon diameter, fiber density, myelin concentration, or the distribution of fiber orientation (Beaulieu 2002; Le Bihan 2003; Jones et al. 2013; Friedrich et al. 2020).

Recent advances in neuroimaging offer promising techniques that allow more differentiated and specific conclusions to be drawn about the microstructure of white matter and the three hypotheses mentioned (Friedrich et al. 2020). Neurite orientation dispersion and density imaging (NODDI; Zhang et al. 2012) and myelin water fraction (MWF) imaging (Laule et al. 2007; MacKay and Laule 2016) both are noninvasive, but take advantage of the unique patterns that water molecules create in different environments.

NODDI utilizes a three-compartment model that differentiates between intra-neurite, extra-neurite, and cerebrospinal fluid (CSF) environments based on a multi-shell high-angular-resolution diffusion imaging protocol (Zhang et al. 2012). While isotropic diffusion occurs mainly in regions with CSF, intracellular compartments are characterized by stick-like or cylindrically symmetrical diffusion, as the water molecules are restricted by the membranes of neurites, and extracellular compartments by hindered diffusion, as there are many cellular membranes of somas and glial cells. The different diffusion properties allow the estimation of NODDI markers as approximations for different aspects of neurite morphology, such as the neurite density index (NDI), which represents the volume fraction of intra-neurite environments, and the orientation dispersion index (ODI), which quantifies the angular variation of neurite dispersion (Zhang et al. 2012). Histological studies supported the validity of the NODDI model (Grussu et al. 2017).

MWF imaging relies on signals from myelin water, as signals from larger molecules such as lipids and proteins (main components of myelin) quickly decay to zero (Laule et al. 2007; MacKay and Laule 2016). Unmyelinated neurons and glial cells have single bilayer membranes, whereas myelinated neurons possess multibilayer membranes, with ∼40% of their mass consisting of compartmentalized water (MacKay and Laule 2016). Although there is currently no method capable to measure the myelin bilayer directly, MWF imaging is considered the method of choice to estimate myelin content *in vivo* (Laule et al. 2007; MacKay and Laule 2016). Studies validated the specificity of MWF imaging mapping the myelin bilayer by comparison with histological results (Laule et al. 2006, 2008, 2016; Baadsvik et al. 2023) and demonstrated that MWF imaging has good reliability (Vavasour et al. 2006; Borich et al. 2013; Meyers et al. 2013; Vargas et al. 2015).

Thus, the question of whether the association between higher FA values and higher intelligence is due to greater axon density, parallel, homogenous fiber orientation distributions, or greater myelination can be answered by associating general intelligence with the corresponding indices NDI, ODI, and MWF. However, there are few to no studies that have used NODDI or MWF imaging in relation to intelligence.

Regarding NODDI, Genç et al. (2018) were the first to analyze the microstructural architecture of intelligence. They showed that higher intelligence was associated with lower NDI and ODI in the gray matter and thus concluded that the neuronal circuitry linked to higher intelligence is structured in a sparse and efficient way (Genç et al. 2018). For white matter, which is more relevant for this paper, Yeung et al. (2023) showed that structural connectomes weighted by NDI or ODI were similarly good at predicting the *g* factor as connectomes weighted by FA. Furthermore, associations between NODDI metrics and individual cognitive functions such as paired associate learning (Coad et al. 2020), episodic memory (Gozdas et al. 2021), or processing speed (Gozdas et al. 2021) have been reported in healthy adults. Callow et al. (2022) found that the ODI of the cerebellar peduncle was significantly associated with fluid, but not crystallized cognition in healthy young adults.

To the best of our knowledge, there is no paper to date that analyzed MWF with regard to general intelligence in healthy adults. Penke et al. (2012) were the first to use a biomarker of myelin, magnetization transfer ratio (MTR), to study intelligence in a sample of healthy older people. They were able to show that MTR correlated significantly with general intelligence. However, although a change in myelin content causes a change in MTR,

MTR is also influenced by other pathological factors (Gareau et al. 2000; Vavasour et al. 2011; MacKay and Laule 2016), so MTR is not as specific to myelin as MWF (Laule et al. 2007; MacKay and Laule 2016). The relation between MWF and cognitive abilities in healthy adults has only been studied for specific cognitive functions such as processing speed (Gong et al. 2023b), executive functions (Gong et al. 2023a), or memory performance (Mendez Colmenares et al. 2024) in middle-aged adults, but not for general intelligence or for young adults. While many studies investigate MWF as a biomarker of human cerebral aging or neurodegenerative diseases (Faulkner et al. 2024), interindividual variability in MWF values also occurs in young adults (Dvorak et al. 2021). In general, MWF increases in the third decade of life, reaches a plateau around the fifth decade of life, and decreases in later decades (Dvorak et al. 2021). Myelin maturation in the brain is protracted, proceeding from caudal to rostral, so that the prefrontal cortex is still subject to myelination in young adulthood, which is associated with the development of higher cognitive functions (Khelfaoui et al. 2024). Although the mechanisms underlying the link between myelination and cognitive development are not yet fully understood, myelin sheaths are crucial for the saltatory conduction of action potentials across axons (Faulkner et al. 2024; Khelfaoui et al. 2024). Thus, myelin plays a key role in increasing conduction velocity and ensuring precise spike timing, both of which are critical for the synchronization and coupling of neuronal ensembles across distributed brain networks (Khelfaoui et al. 2024). On a larger scale, myelin architecture in the human brain is closely linked to functional brain networks (Hunt et al. 2016). Myelin plasticity further enables adaptive fine-tuning of conduction delays in response to neuronal activity (Khelfaoui et al. 2024), suggesting that even subtle variations in myelin properties could influence the efficiency of information transfer and network communication, which in turn could impact intelligent performance.

To better understand the microstructural architecture of general intelligence, our study aimed to analyze the relation between general intelligence and NDI, ODI, and MWF within the same sample, with all indices extracted from the same 64 white matter fiber tracts. To further complete the picture, we did not limit our analyses to the relation between the brain and intelligence, but included genes and directly considered the triad between genes, the brain, and behavior via mediation analyses.

General intelligence is a highly heritable trait, with inherited differences in desoxyribonucleic acid (DNA) sequence explaining for about half of the variance in intelligence across all ages (Haworth et al. 2010; Polderman et al. 2015; Plomin and von Stumm 2018; Deary et al. 2022). However, heritability of intelligence is not due to few individual genes, but results from thousands of genetic variants, mostly single nucleotide polymorphisms (SNPs), whose small effects on the variation of intelligence add up (Plomin and von Stumm 2018; Deary et al. 2022). Polygenic scores (PGS) offer the possibility to account for this highly polygenic architecture by aggregating the effects of different SNPs across the genome into a summarized measure (Choi et al. 2020). Results of genome-wide association studies (GWASs), used to identify which SNPs throughout the genome are statistically associated with a particular trait, show which of the two alleles for a SNP is positively associated with the trait (called increasing allele) and provide effect sizes for each SNP (Plomin and von Stumm 2018; Deary et al. 2022). A PGS is constructed by summing the number of increasing alleles associated with intelligence across SNPs and weighting them by the respective effect size obtained from GWAS (Plomin and von Stumm 2018; Deary et al. 2022). PGS for intelligence, derived from one of the largest GWAS to date based on 269,867 individuals, explain up to 5.2% of variance in general intelligence in independent samples (Savage et al. 2018).

Genetic correlations show that the genetic variants associated with intelligence are partially consistent with those associated with brain structure (Davies et al. 2018; Deary et al. 2022). White matter microstructure has been shown to be highly polygenic as well and positive genetic correlations with higher intelligence have been identified (Zhao et al. 2021a, 2021b; Deary et al. 2022; Fan et al. 2022). The gene sets significantly associated with intelligence include neurogenesis, neuron differentiation, central nervous system neuron differentiation, regulation of nervous system development, positive regulation of nervous system development, and regulation of synapse structure or activity (Savage et al. 2018). While other GWAS analyses on intelligence reported similar gene sets (Davies et al. 2018; Hill et al. 2019), gene sets such as myelin sheath or regulation of myelination were not found to be significantly related to intelligence in any study. Lee et al. (2018), who performed a large GWAS on educational attainment, also found no gene sets related to glial cells that were positively enriched and concluded that differences in cognition may not necessarily be driven by differences in myelination and thus transmission speed.

Mediation analyses represent a useful tool to investigate the relation between PGS for general intelligence (PGS_{GI}), microstructural white matter indices (NDI, ODI, and MWF), and general intelligence. However, there are only few mediation studies in healthy adults investigating the relation between genes, the brain, and intelligence, and those that exist have focused their analyses on mediation effects of total brain volume, surface area, cortical thickness, white matter fiber network efficiency, and functional efficiency (Elliott et al. 2019; Lett et al. 2020; Mitchell et al. 2020; Genç et al. 2023; Williams et al. 2023). Although Genç et al. (2023) found the white matter fiber network efficiency of two brain areas to be mediators regarding the effects of PGS on general intelligence using data from the same sample, they did not include white matter microstructure indices in their analyses, and to the best of our knowledge, other studies have not used such indices in mediation analyses in healthy adults either.

To summarize, NODDI and MWF imaging, with their indices NDI, ODI, and MWF, offer opportunities to analyze the microstructural architecture of intelligence on a new level and draw more differentiated and specific conclusions regarding the question whether the association between higher FA values and higher intelligence is due to greater axon density (NDI), parallel, homogenous fiber orientation distributions (ODI), or greater myelination (MWF). While these opportunities have only been used selectively for NODDI, to our knowledge there is no study that has investigated the relation between MWF and general intelligence in healthy young adults, so we performed this analysis here for the first time. Furthermore, we expanded the existing literature on mediation analyses regarding the relations between genes, the brain, and intelligence to include white matter microstructure. We analyzed the effects of PGS_{GI} on general intelligence and tested the mediating role of NDI, ODI, and MWF of 64 white matter fiber tracts in a large sample of at least 500 individuals. Thus, this study presents the first mediation analyses that give insight whether white matter microstructure indices provide a biological pathway through which our genetics influence general intelligence.

Materials and methods

Participants

The sample consisted of 557 adults with a mean age of 27.33 years (SD = 9.43 years; range: 18 to 75 years, 503 right-handers), including 283 men (mean age = 27.71 years; SD = 9.86 years,

246 right-handers) and 274 women (mean age = 26.94 years; SD = 8.96 years, 257 right-handers). It has previously been used to investigate relations between genetic variability, brain properties, and intelligence (Genç et al. 2023). Handedness was assessed using the Edinburgh Handedness Inventory (Oldfield 1971). Participants were mostly university students of different majors (mean years of education = 17.14 years; SD = 3.12 years), who were either financially compensated for their participation or received course credits. Individuals who had insufficient German-language skills or reported having done any of the employed intelligence tests within the last 5 years were excluded from the study. Health status was assessed by a self-report questionnaire. Individuals were also not admitted to the study if they or any of their close relatives suffered currently or in the past from neurological and/or mental illnesses. The study protocol was approved by the Local Ethics Committee of the Faculty of Psychology at Ruhr University Bochum (vote Nr. 165). All participants gave written informed consent and were treated according to the Declaration of Helsinki.

Acquisition and analysis of behavioral data

General intelligence was assessed by the use of four paper-and-pencil tests. The tests were conducted in a quiet and well-lit room.

Intelligenz-Struktur-Test 2000 R

The Intelligenz-Struktur-Test 2000 R (I-S-T 2000 R; Liepmann et al. 2007) is a well-established German intelligence test battery, requiring about 2.5 h to complete. It evaluates various aspects of intelligence as well as general intelligence and is largely comparable to the internationally established Wechsler Adult Intelligence Scale Fourth Edition (Erdodi et al. 2017). The majority of included cognitive test items are presented in multiple-choice format. The test consists of a basic and an extension module. Within the basic module, verbal, numerical, and figural abilities are each assessed by three different mental reasoning tasks of 20 items. Verbal intelligence is assessed by tasks in which participants must complete sentences (IST_SEN), find analogies (IST_ANA), and recognize similarities (IST_SIM). Numerical intelligence is assessed by tasks involving arithmetic calculations (IST_CAL), number series (IST_SER), and mathematical equations to which arithmetic signs need to be added (IST_SIG). Figural intelligence is assessed by tasks in which participants must select and reassemble parts of a cut-up figure (IST_SEL), mentally rotate and match three-dimensional objects (IST_CUB), and solve matrix-reasoning problems (IST_MAT). In addition, retention (IST_RET) is assessed by 10 verbal and 13 figural items. Here, participants must memorize series of words or figure pairs. The extension module comprises 84 multiple-choice questions on six knowledge facets (art/literature, economy, geography/history, mathematics, science, and daily life) and measures general knowledge (IST_KNO). Reliability estimates (Cronbach's α) are between 0.88 and 0.96 for subtests and composite scores. The recent norming sample consists of ~5,800 individuals for the basic module and 661 individuals for the extension module. The age range in the norming sample is between 15 and 60 years, and both sexes are represented equally (Liepmann et al. 2007).

BOMAT-Advanced Short

The Bochumer Matrizentest (BOMAT; Hossiep et al. 2001) is a nonverbal German intelligence test which is widely used in neuroscientific research (Hossiep et al. 2001; Jaeggi et al. 2008; Oelhafen et al. 2013; Genç et al. 2018, Genç et al. 2019; Fraenz et al. 2021; Genç et al. 2021) and whose structure resembles that of the well-established Raven's Advanced Progressive Matrices (Raven et al. 1990). Within the framework of our study, we employed the advanced short version, which is characterized by high discriminatory power in samples with generally high intellectual abilities, thus avoiding possible ceiling effects (Genç et al. 2018, 2019). The test comprises two parallel forms with 29 matrix-reasoning items. Each item shows a 5-by-3 matrix composed of elements arranged according to a specific but unspecified rule. One field within the matrix is empty and needs to be filled with one of six provided elements that follows the rule. The participants were assigned to one of the two parallel forms and had to complete as many matrices as possible within a time limit of 45 min. Split-half reliability of the BOMAT is 0.89, Cronbach's α is 0.92, and reliability between the parallel forms is 0.86. The recent norming sample consists of ~2,100 individuals with an age range between 18 and 60 years and equal sex representation (Hossiep et al. 2001).

Bochumer Wissenstest

The Bochumer Wissenstest (BOWIT; Hossiep and Schulte 2008) is a German general knowledge questionnaire. It assesses 11 different knowledge facets from two major domains. The four facets biology/chemistry, mathematics/physics, nutrition/exercise/health, and technology/electronics are assigned to the scientific-technical knowledge domain. The social and humanistic knowledge domain includes seven facets: arts/architecture, civics/politics, economies/laws, geography/logistics, history/archaeology, language/literature, and philosophy/religion. The BOWIT is available in two parallel test forms, in which each knowledge facet is represented by 14 multiple-choice questions. To measure general knowledge as precisely as possible, all participants had to complete both test forms, resulting in 308 items. The BOWIT shows reliability estimates >0.90: split-half reliability is reported as 0.96, Cronbach's α 0.95, test–retest reliability 0.96, and parallel-form reliability 0.91. The recent norming sample consists of ~2,300 individuals with an age range between 18 and 66 years and equal sex representation (Hossiep and Schulte 2008).

Zahlenverbindungstest

The Zahlenverbindungstest (Oswald and Roth 1987) is a trail-making test used to assess the cognitive processing speed of both children and adults. After completing two short sample tasks, four main tasks are assessed. Here, participants connect numbers from 1 to 90 according to a specific rule as fast as possible. The processing times for the four tasks are averaged to obtain an overall measure of processing speed. The reliability across the four tasks is reported as 0.95 in adults. The 6-month retest-reliability is reported to be between 0.84 and 0.90. The recent norming sample consists of 2,109 individuals with an age range between 8 and 60 years and equal sex representation (Oswald and Roth 1987).

Computation of the general intelligence factor, *g*

We computed the general intelligence factor to provide a comparable and robust measure of intelligence. When included tests measure intelligence broadly enough, *g* factors derived from different test batteries are statistically equivalent (Johnson et al. 2004, 2008). As described in Stammen et al. (2023), we used the intelligence test scores to compute *g* factor scores for every participant. After regressing age, sex, age∗sex, age^2, and age^2∗sex from the test scores, we used the standardized residuals to develop a hierarchical factor model via exploratory factor analysis. Subsequently, we performed confirmatory factor analysis to assess model fit using the chi-square (χ^2) statistic as

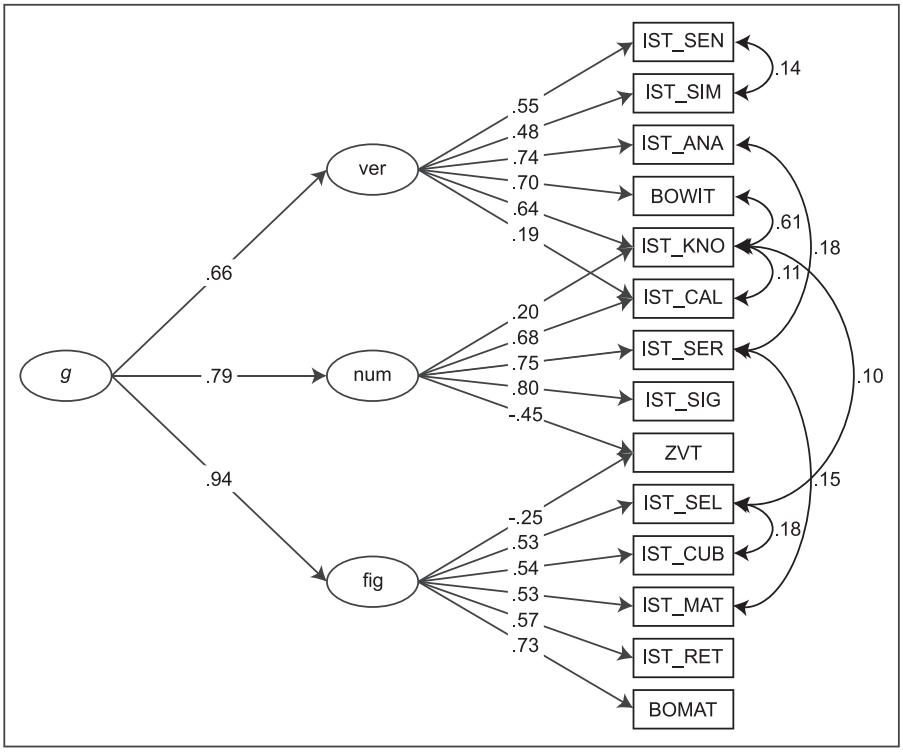

Fig. 1. Confirmatory factor analytic model. *g* = general factor of intelligence, ver = verbal intelligence as broad cognitive domain, num = numerical intelligence as broad cognitive domain, fig = figural intelligence as broad cognitive domain, IST_SEN = subtest sentence completion of the I-S-T 2000 R, IST_SIM = subtest similarities of the I-S-T 2000 R, IST_ANA = subtest analogies of the I-S-T 2000 R, BOWIT = Bochumer Wissenstest, IST_KNO = parameter knowledge of the I-S-T 2000 R, IST_CAL = subtest calculations of the I-S-T 2000 R, IST_SER = subtest number series of the I-S-T 2000 R, IST_SIG = subtest numerical signs of the I-S-T 2000 R, ZVT = Zahlenverbindungstest, IST_SEL = subtest figure selection of the I-S-T 2000 R, IST_CUB = subtest cubes of the I-S-T 2000 R, IST_MAT = subtest matrices of the I-S-T 2000 R, IST_RET = parameter retentiveness of the I-S-T 2000 R, BOMAT = Bochumer Matrizentest.

well as the fit indices root mean square error of approximation (RMSEA), standardized root mean square residual (SRMR), Comparative Fit Index (CFI), and Tucker–Lewis Index (TLI). The evaluation of model fit yielded good fit. Although the chi-square (χ^2) statistic assessing the magnitude of discrepancy between the model-implied variance–covariance matrix and the empirically observed variance–covariance matrix (Hu and Bentler 1999) was significant ($\chi^2(64) = 127.97$, $P < 0.001$), this did not itself show poor model fit since the chi-square (χ^2) statistic is a direct function of sample size meaning that the probability of rejecting any model increases with greater sample size (Jöreskog 1969; Bentler and Bonett 1980). The other fit indices (RMSEA = 0.042, SRMR = 0.033, CFI = 0.979, and TLI = 0.969) were all acceptable as values of RMSEA and SRMR <0.05 and values of CFI and TLI >0.97 are considered good (Hu and Bentler 1999). Based on the postulated confirmatory factor model shown in Fig. 1, we calculated regression-based *g* factor scores for every participant, winsorizing outliers (Wilcox 1997). We examined the *g* factor score distribution and limited data points that laid far enough above or below where the data began to cohere to distort regression lines to those levels. To ensure that these restrictions did not substantially alter the overall distribution shape, we assessed both skew and kurtosis.

Intelligence level

Unfortunately, it is not possible to link *g* to the intelligence quotient (IQ) scale. Nevertheless, we used norming data of some tests to estimate the intelligence level. Norming data of the subtests of the I-S-T 2000 R revealed that the sample's mean IQ was 115 (SD = 13.0). The fact that our sample had a mean score 1 SD above average may have impacted the associations with the polygenic scores and the white matter fiber tracts' microstructure.

DNA sampling and genotyping

We used exfoliated cells that were brushed from the participants' oral mucosa for genotyping. DNA isolation was done with QIAamp DNA mini Kit (Qiagen GmbH, Hilden, Germany). Genotyping was executed with the Illumina Infinium Global Screening Array 1.0 with multi-disease (MD) and Psych content (Illumina, San Diego, CA, USA) at the Life & Brain facilities (Bonn, Germany) and yielded 745,747 SNPs. Filtering was conducted with PLINK 1.9 (Chang et al. 2015; Purcell and Chang n.d.) by eliminating all SNPs with a minor allele frequency (MAF) of < 0.01, deviating from Hardy–Weinberg equilibrium (HWE) with a *p*-value of $< 1*10^{-6}$, and missing data > 0.02. Participants were removed with > 0.02 missingness, sex-mismatch, and heterozygosity rate > |0.2|. A high quality (HWE $p > 0.02$, MAF > 0.2, missingness = 0) and linkage disequilibrium pruned ($r^2 = 0.1$) SNP set was used for filtering for relatedness and population structure. In pairs of related subjects, pi hat > 0.2 was used to exclude subjects randomly. Principal components (PCs) were generated to control for population stratification. Participants who deviated more than |6| SD from the mean on at least one of the first 20 PCs were classified as outliers and excluded. The final data set consisted of 519 participants and 498,760 SNPs. The samples' filtered genotype data were submitted for imputation to the Michigan Imputation server (Das et al. 2016) using the European population of the Haplotypes Reference Consortium panel (r1.1 2016; hg19) and a R^2 filter of 0.3. We chose Eagle 2.4 for phasing and Minimac4 for imputation. After a final MAF <0.01 filtering step, 5,338,876 SNPs were available for analysis.

Polygenic scores

We generated genome-wide PGS for each participant using publicly available summary statistics for general intelligence ($n = 269{,}867$; Savage et al. 2018). General intelligence PGS (PGS_{GI}) were computed as weighted sums of each subject's trait-associated alleles across all SNPs using PRSice 2.1.6 (Choi and O'Reilly 2019). Specifically, we computed best-fit PGS_{GI} that showed the strongest association with general intelligence (Genç et al. 2021, 2023). We applied a p-value threshold (PT) for the inclusion of SNPs that was chosen empirically by carrying out multiple linear regression analyses iteratively for the range of PT $5*10^{-8}$ to 0.5 in steps of $5*10^{-5}$. The predictive power of the PGS_{GI} was assessed by the "incremental R^2" statistic (Lee et al. 2018). Incremental R^2 indicates the increase in the coefficient of determination (R^2) when the PGS_{GI} is added as a covariate to a regression model predicting general intelligence together with a number of baseline control variables (here: age, sex, and the first four PCs of population stratification). Linear parametric methods were chosen for all statistical analyses in PRSice. Testing was two-tailed with an α-level of $p < 0.05$. The PGS_{GI} with the greatest predictive power, explaining the maximum amount of g variance, was chosen for further analyses. Since this approach involves parameter optimization, the best-fit model's R^2 and p-value are overfitted. Nevertheless, the PGS_{GI} explained 4.37% of variance of general intelligence ($p_{corrected} < 0.001$) in our sample at a SNP p-value threshold of 0.0062, which resulted in 4,659 SNPs being included in the calculation of PGS_{GI} and is consistent with previous findings (Genç et al. 2021, 2023). The p-value of the multiple regression was adjusted for type I error using PRSice 2.1.6's permutation-based approach, which involves repeating the procedure 10,000 times while shuffling the phenotype data in each iteration (Choi and O'Reilly 2019). Additionally, overfitting only affects the direct path between PGS_{GI} and g, whereas indirect pathways ($PGS_{GI} \sim$ microstructural index and microstructural index $\sim g$) are unaffected, as they were not involved in the P-value threshold optimization. A distribution of the PGS_{GI} is shown in Supplementary Fig. S1.

Acquisition and analysis of imaging data

All images were collected within one session on a Philips 3T Achieva scanner at the Bergmannsheil Hospital in Bochum, Germany, using a 32-channel head coil.

Multi-shell diffusion-weighted imaging

For the analysis of NODDI coefficients, a diffusion-weighted three-shell image was acquired using echo-planar imaging) with the following parameters: time repetition (TR) = 7,652 ms; time echo (TE) = 87 ms; flip angle = 90°; 60 slices; matrix size = 112 × 112; voxel size = 2 × 2 × 2 mm; parallel imaging sensitivity encoding (SENSE) factor = 2; direction of acquisition = anterior–posterior (AP). Diffusion weighting was uniformly distributed along 120 directions (20 directions with a b-value of 1,000 s/mm^2; 40 directions with a b-value of 1,800 s/mm^2; 60 directions with a b-value of 2,500 s/mm^2). We used the multiple acquisitions for standardization of structural imaging validation and evaluation toolbox (MASSIVE toolbox; Froeling et al. 2017) to generate all diffusion directions within and between shells non-collinear to each other. Additionally, eight volumes with no diffusion weighting (b-value of 0 s/mm^2) were acquired for the purpose of motion correction and computation of NODDI coefficients. Diffusion-weighted data were collected with reversed phase-encode directions, resulting in pairs of images with distortions going in opposite directions. Total acquisition time was 18 min.

Diffusion-weighted data were prepared for NODDI coefficients via a preprocessing pipeline comprising the following steps. First, images were corrected for signal drift (Vos et al. 2017) using ExploreDTI (Leemans et al. 2009). Second, we utilized the topup command from the Oxford Centre for Functional Magnetic Resonance Imaging of the Brain's (FMRIB's) Software Library (FSL) toolbox (version 6.0.7.7; https://fsl.fmrib.ox.ac.uk/fsl/docs/#/; Andersson et al. 2003; Smith et al. 2004) to estimate the susceptibility-induced off-resonance field based on pairs of images with opposite phase-encode directions. Third, the topup output was used in combination with the eddy command (Andersson and Sotiropoulos 2016), which is also part of the FSL toolbox (Smith et al. 2004), to correct for susceptibility, eddy currents, and head movement. Importantly, we also performed outlier detection during this step to identify slices where signal had been lost due to head movement during the diffusion encoding (Andersson et al. 2016).

We used the Microstructure Diffusion Toolbox (MDT; https://github.com/robbert-harms/MDT; Harms et al. 2017; Harms and Roebroeck 2018) to compute NODDI coefficients. The advantage of MDT in comparison to the original NODDI toolbox in MATLAB (Zhang et al. 2012) is that MDT is utilized on graphics processing unit cores and thus dramatically reduces estimation time. It is even faster than the AMICO toolbox (Daducci et al. 2015) we used in previous studies (Genç et al. 2018; Friedrich et al. 2020; Schlüter et al. 2022). By default, MDT uses the Offset Gaussian likelihood model and the Powell conjugate-direction optimization routine (Powell 1964) for maximum-likelihood estimation (Harms et al. 2017). Specifically, we employed the implemented, three-part NODDI model of Zhang et al. (2012) that distinguishes between intra-neurite, extra-neurite, and CSF environments. The NODDI technique is based on a two-level approach. First, the proportion of free-moving water within each voxel is analyzed based on the diffusion signal obtained by the multi-shell high-angular-resolution imaging protocol (Jespersen et al. 2010, 2012; Zhang et al. 2012; Billiet et al. 2015). This proportion is called isotropic volume fraction and reflects the amount of isotropic diffusion with Gaussian properties that mainly characterizes regions with a focus on CSF. Second, the remaining portion of the diffusion signal is assigned to one of the complementary fractions, either intra- or extra-neurite environment (Jespersen et al. 2010, 2012; Zhang et al. 2012). The amount of intra-neurite environments is quantified as the intra-neurite volume fraction or NDI. The intracellular compartment represents the amount of stick-like or cylindrically symmetric diffusion that occurs when water molecules are confined by the membranes of neurites and resembles the proportion of axonal density in white matter as shown by comparison with light microscopy and electron microscopy in histological samples (Jespersen et al. 2010). Extra-neurite environments in the white matter are usually full of various types of glial cells and therefore characterized by hindered diffusion (Jespersen et al. 2010, 2012; Zhang et al. 2012). A NODDI's summary statistic is the neurite ODI that quantifies angular variation of neurite orientation (Zhang et al. 2012). ODI is a measure of tortuosity that couples the intra-neurite space and the extra-neurite space and thus leads to an alignment or dispersion of the axons in the white matter (Zhang et al. 2012; Billiet et al. 2015). Examples of NDI and ODI coefficient maps from a representative individual are illustrated in Fig. 2 (upper-left corner).

Myelin water imaging

A previously published 32 multi-echo (ME) three-dimensional (3D) turbo gradient spin echo (GRASE) sequence with refocusing

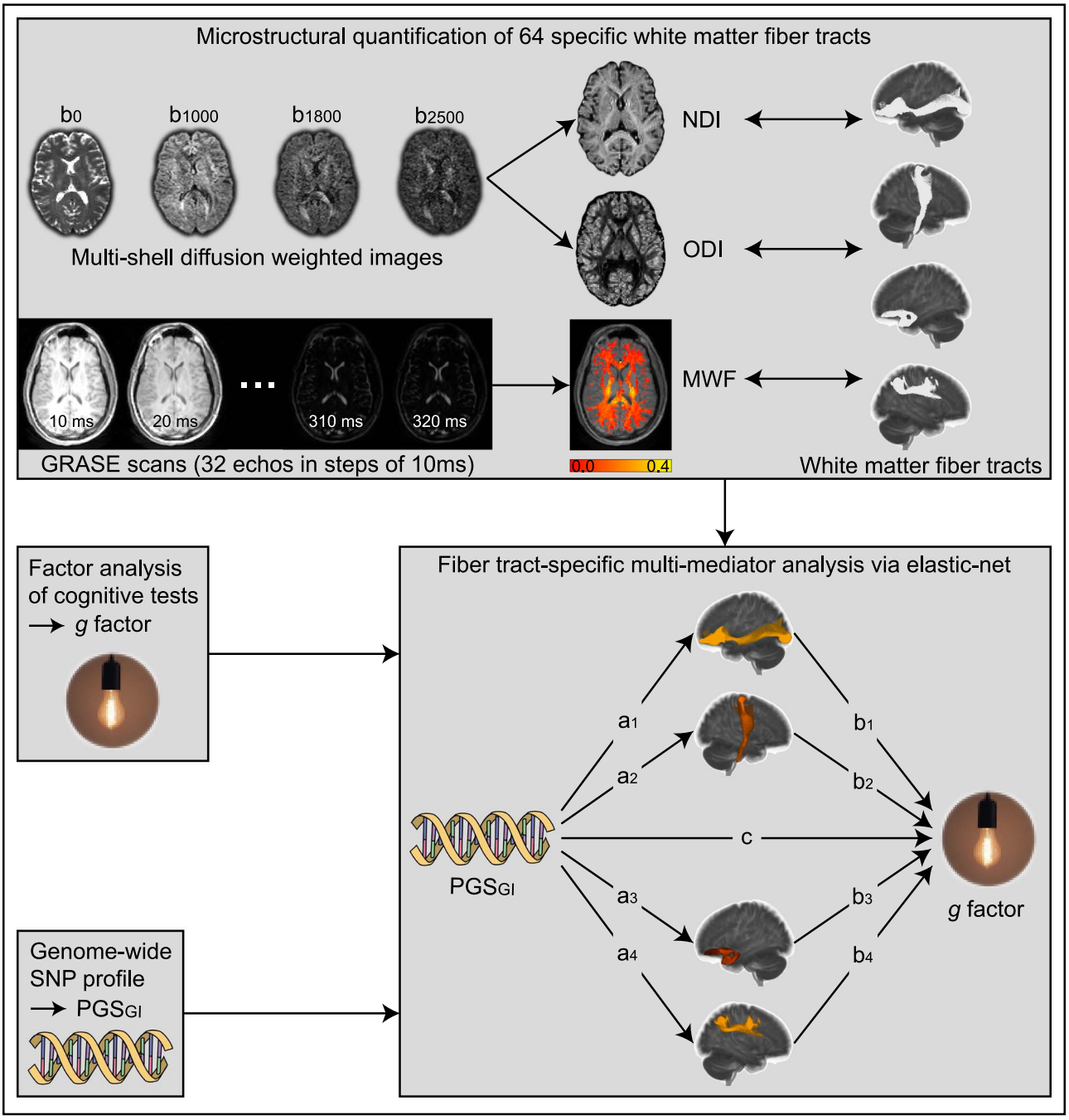

Fig. 2. Processing steps of neuroimaging and statistical analyses. Multi-shell diffusion-weighted images were used to compute neurite density and neurite orientation dispersion indices (NDI and ODI). Images resulting from the three-dimensional (3D) multi-echo (ME) turbo gradient spin echo (GRASE) sequence were used to compute the myelin water fraction (MWF) for each voxel. In total, 64 white matter fiber tracts provided by the population-based HCP-1065 probabilistic tract atlas (Yeh et al. 2018; Yeh 2022) were downloaded, transformed in the respective native space, and served as anatomical references for the extraction of the microstructural properties NDI, ODI, and MWF. Fiber tract–specific multi-mediator analyses were performed via elastic-net regression for each microstructural property. General intelligence, quantified by the factor of general intelligence *g*, was the dependent variable, while the polygenic score of general intelligence (PGS_{GI}) was the independent variable. NDI, ODI, or MWF values of each white matter fiber tract served as mediators.

angle sweep (Prasloski et al. 2012; Billiet et al. 2015; Ocklenburg et al. 2019; Friedrich et al. 2020) was acquired with the following parameters: TR = 800 ms; TE = 32 echoes at 10 ms echo spacing (ranging from 10 to 320 ms); 60 slices; partial Fourier acquisition in both phase encoding directions; matrix size = 112 × 112; voxel size = 2 × 2 × 2 mm; parallel imaging SENSE factor = 2; direction of acquisition = right–left (RL). Total acquisition time for this sequence was 8 min.

To assess the myelin content of the white matter fiber tracts, we used an in-house algorithm (Ocklenburg et al. 2019; Friedrich et al. 2020) written in MATLAB (version 8.5.0.197613 (R2015a); The MathWorks Inc., Natick, MA) to construct parameter maps representing the MWF for each voxel based on the 3D ME-GRASE sequence. As described in Prasloski et al. (2012) in detail, this algorithm analyzed the ME decay curves voxel by voxel using multicomponent T2 analysis with simultaneous correction for

contamination of the decay curves by stimulated echoes resulting from B1 inhomogeneity and imperfect refocusing pulses. Voxelwise ME decay curves were acquired from the 3D ME-GRASE images and transformed into a continuous T2-distribution by applying a regularized non-negative least squares approach (Whittal and MacKay 1989; Whittall et al. 1997). We used an extended phase graph algorithm to take possible stimulated echoes due to non-ideal refocusing pulse flip angles into consideration (Hennig 1988; Hennig et al. 2003; Prasloski et al. 2012). During the fitting procedure, a regularization factor of 1.02 was applied to increase robustness of the ill-posed fitting problem and to assure smooth T2 amplitude distributions. T2 distributions were generated using 101 logarithmically spaced exponential decay base functions for echo decay with T2 values ranging from 0.01 to 2 s. From the T2 distributions, the MWF was calculated for each voxel as the signal integral fraction between 10 and 40 ms relative to the total T2 distribution integral (area under the curve). This resulted in whole-brain MWF maps for each subject, as exemplified in Fig. 2 (upper-left corner).

Quantification of microstructural properties in white matter fiber tracts

We used 64 white matter fiber tracts provided by the population-based HCP-1065 probabilistic tract atlas (Yeh et al. 2018; Yeh 2022), from the official website (https://brain.labsolver.org/hcp_trk_atlas.html) as NIfTI files. This atlas displays for 64 different fiber tracts for each voxel the probability of being part of the respective white matter fiber tract compiled from the tractography of 1,065 subjects (Yeh 2022), with underlying data ("1200 Subjects Data Release") provided by the Human Connectome Project (HCP), WU-Minn Consortium (Principal Investigators: David van Essen and Kamil Ugurbil; 1U54MH091657), funded by the 16 United States National Institutes of Health (NIH) and Centers supporting the NIH Blueprint for Neuroscience Research and by the McDonnell Center for Systems Neuroscience at Washington University (Van Essen et al. 2013). In a first step, fiber tracts' NIfTI files were processed using DSI Studio (https://dsi-studio.labsolver.org; Yeh 2022; Yeh et al. 2018). We resized the dimensions to match the International Consortium for Brain Mapping (ICBM) 2009a Nonlinear Asymmetric NIfTI template file (Fonov et al. 2011). The threshold for the fiber tracts' probability was set at 0.50 to include only voxels that were part of major white matter tracts in at least half of the sample and exclude peripheral voxels that are more susceptible to intra- and intersubjective variability. We then binarized the fiber tracts and transformed them into a common space via FMRIB's Linear Image Registration Tool (FLIRT; Greve and Fischl 2009; Jenkinson et al. 2002; Jenkinson and Smith 2001). We chose the template MNI152_T1_1mm_brain within FSL, which is derived from 152 structural images that have been nonlinearly registered into the common Montreal Neurologic Institute (MNI) 152 standard space ($1 \times 1 \times 1$ mm). Starting from the MNI 152 standard space, we used FMRIB's Nonlinear Image Registration Tool (Andersson et al. 2007) to nonlinearly transform the fiber tracts into the native space of the diffusion-weighted images as well as into the 3D ME-GRASE image space. Each participant's aligned fiber tracts served as anatomical references from which NODDI coefficients and MWF coefficients were extracted (see Fig. 2, upper-right corner).

Statistical analyses

All statistical analyses were conducted in R Studio (version 2022.12.0.353; RStudio Team 2022) with R version 4.2.2 (2022 October 31; R Core Team 2022). The final data set included 501 participants (242 women; mean age = 27.30 years; SD = 9.22 years; 455 right-handers) as we only had usable genetic data from 519 subjects and analyzable MWF data from 539 subjects. Data points were treated as outliers if they deviated more than three interquartile ranges from the respective variable's group mean (PGS_{GI}, mean NDI of all 64 fiber tracts, mean ODI of all 64 fiber tracts, mean MWF of all 64 fiber tracts). In such cases, all data from the corresponding participant were removed from analysis. No subjects were excluded from analyses concerning PGS_{GI}, NDI, MWF, and g, while one participant had to be excluded for analyses concerning PGS_{GI}, ODI, and g (500 remaining subjects).

To investigate whether a set of specific white matter fiber tracts mediates the association between PGS_{GI} (independent variable) and general intelligence (dependent variable), we used exploratory mediation analysis by regularization (see Fig. 2, lower-right corner), an approach developed to identify a set of mediators from a large pool of potential mediators without testing specific theory-based and predefined hypotheses (Serang et al. 2017; Serang and Jacobucci 2020). Confirmatory theory-based approaches in general test models that have been specified in advance, rely on P-values to test statistical significance, require correction for multiple comparisons with respect to many possible mediators, and tend to overfit the data in the regression context, resulting in less generalizable solutions (Babyak 2004; McNeish 2015; Serang et al. 2017). In contrast, exploratory mediation analysis by regularization is based on regularization and penalization techniques (Serang et al. 2017), such as the least absolute shrinkage and selection operator (lasso; Tibshirani 1996). It aims to improve the generalization ability of a model and prevent overfitting (Tian and Zhang 2022) by applying a penalty to effect sizes, resulting in small effect sizes being pushed to zero, leaving only strong non-zero effects.

A detailed explanation of this machine learning approach is provided by Serang et al. (2017). In short, this approach is based on a two-stage process. First, all potential mediators of interest are included in a multiple mediator model which is then fit using lasso resulting in the corresponding regression weights a and b being penalized (Ammerman et al. 2018). The tuning parameter of the penalty term, lambda, is typically selected by testing a range of candidate values via k-fold cross-validation, an approach primarily utilized to prevent overfitting (Serang et al. 2017). The data are divided into k different subsets. The model is then trained on $k-1$ subsets, while the kth subset is used as the testing set. This is repeated k times so that each subset serves as the testing set once. The value of lambda chosen is the one with the best fit resulting in the lowest prediction error. Since the mediation effect of a mediator corresponds to the product of the regression parameters a and b, the effect becomes zero if either the a or b parameter of a mediator is regularized to zero by the penalty. Those mediators with non-zero values of a and b after regularization will be considered selected as mediators. While this approach makes it possible to eliminate mediators with small effect sizes, it also means that the effect sizes of the selected mediators are close to zero due to penalization and are therefore underestimated. To eliminate this potential bias, the second step is to refit the model using only the selected mediators without any penalization (Serang et al. 2017). This allows unbiased estimates of effect sizes to be obtained (Serang and Jacobucci 2020).

Instead of using lasso regression, we employed elastic-net regression in our analyses. Elastic-net regression results from the combination of ridge regression (Hoerl and Kennard 2000) and lasso regression (Tibshirani 1996) and is thus another form of regularized regression (Zou and Hastie 2005) allowing better accuracy of prediction on future data and interpretation of the model due to parsimony in contrast to ordinary least squares

estimates. While lasso regression can penalize a parameter to zero and is therefore suitable for models where many variables are assumed to have little or no effect on the dependent variable, ridge regression can only asymptotically shrink parameters toward zero and is therefore suitable for models where most variables are assumed to have a considerable effect on the dependent variable. Elastic-net regression is an useful approach when there are no clear, predefined hypotheses for all variables (Zou and Hastie 2005). Unlike lasso regression, which tends to randomly select only one variable from a group of variables with high correlations between them, elastic-net regression outperforms lasso as it can select groups of correlated variables (Zou and Hastie 2005). The latter was an important argument in our decision to use elastic-net regression instead of lasso regression.

We used the *xmed* function from the *regsem* package (Serang et al. 2017; Serang and Jacobucci 2020; Jacobucci et al. 2022). All variables were standardized and residualized for age, sex, age∗sex, age^2, age^2∗sex, and the first four PCs of population stratification. Age, sex, age^2, and their interaction effects were used as control variables, as many studies have shown age- and sex-dependent changes in microstructural properties as well as myelination (Cox et al. 2016; Kodiweera et al. 2016; Bouhrara et al. 2020; Buyanova and Arsalidou 2021; Lawrence et al. 2021; Herlin et al. 2024). The first four PCs of population stratification were added to control the variability of the genetic origin of the sample (Price et al. 2006). We calculated three mediation models, where PGS_{GI} was always the independent variable, the NDI, ODI, or MWF values of the 64 white matter fiber tracts each yielded the 64 mediators, and *g* was always the dependent variable. For all mediation models, the number of cross-validation subsets was set to $k = 80$, the threshold for detecting non-zero mediation effects was set to 0.001 (default), and the type of regression was set to elastic-net. All coefficients were re-estimated with *lavaan* (Rosseel 2012) to ensure unbiased effect sizes.

In addition to the mediation effects, we were also interested in the direct effects of PGS_{GI} on the NODDI and MWF brain properties as well as the direct effects of the NODDI and MWF brain properties on intelligence (path *a* and path *b*). To identify variables with non-zero effects within path *a* and path *b* regressions, we followed a similar approach and set the threshold for detecting non-zero effects to 0.01 (Genç et al. 2023). This threshold was chosen a little more liberally since mediation effects are considerably smaller due to the multiplication of the regularized parameters *a* and *b* with values <1. Again, all coefficients were re-estimated with *lavaan* (Rosseel 2012) to ensure unbiased effect sizes.

Results

Neurite density index

The results of the multiple mediator analysis via elastic-net showed that PGS_{GI} was associated with the NDI of 28 white matter fiber tracts (see Fig. 3 and Supplementary Table S1). All effects were positive, indicating that higher PGS_{GI} is associated with higher NDI (path *a*) and thus higher axonal packing density. Furthermore, the NDI of 18 white matter fiber tracts was linked to the *g* score (path *b*). The association was positive for 12 white matter fiber tracts and negative for the remaining 6 fiber tracts. A total of six white matter fiber tracts partially mediated the effects of PGS_{GI} on general intelligence (path *a*∗*b*). While the five white matter fiber tracts middle longitudinal fasciculus (left hemisphere), cingulum parahippocampal parietal (right hemisphere), uncinate fasciculus (left hemisphere), cingulum parahippocampal parietal (left hemisphere), and superior longitudinal fasciculus 3 (right hemisphere) showed positive mediation effects, one white matter fiber tract, namely, frontal aslant tract (left hemisphere), showed a negative mediation effect. The total effect of PGS_{GI} on general intelligence (path *c*) was estimated at $c = 0.207$. After accounting for the indirect pathways through white matter microstructure, the direct effect (path *c*′) was slightly reduced to $c' = 0.201$, indicating partial mediation.

Neurite orientation dispersion index

For the ODI metric, the elastic-net analysis showed that there was an association between PGS_{GI} and the tracts' ODI values in 16 white matter fiber tracts (see Fig. 4a and Supplementary Table S2). As for NDI, all effects were positive, indicating that higher PGS_{GI} is associated with higher ODI (path *a*). Higher ODI indicates a cytoarchitecture with highly dispersed neurites. The multiple mediator analysis revealed no white matter fiber tracts that showed a significant association between the tracts' ODI values and general intelligence (path *b*). Consequently, no mediators (path *a*∗*b*) for the association between PGS_{GI} and *g* could be identified.

Myelin water fraction

PGS_{GI} was associated with the tracts' MWF values in four white matter fiber tracts, of which two exhibited positive effects and two exhibited negative effects (see Fig. 4b and Supplementary Table S3). Higher PGS_{GI} was linked to higher MWF values of the corticopontine tract occipital in the left hemisphere and the reticulospinal tract in the right hemisphere, while higher PGS_{GI} went along with lower MWF values of the cingulum parahippocampal in the left hemisphere and the parietal aslant tract in the right hemisphere. Higher MWF indicates higher myelin content and thus greater myelination. As for ODI, the multiple mediator analysis revealed no white matter fiber tracts that showed a significant association between the tracts' MWF values and general intelligence (path *b*), and thus no mediators (path *a*∗*b*) for the relation between PGS_{GI} and *g* could be identified.

Discussion

The relation between FA values and intelligence has often been demonstrated, but it is still unclear whether it is due to greater axon density, parallel, homogenous fiber orientation distributions, or greater myelination. Using NODDI and MWF imaging data, we addressed this question and analyzed the microstructural architecture of intelligence in more detail. Furthermore, we were interested whether white matter microstructure indices are involved in the biological pathway that links genetic disposition to phenotype. Thus, we conducted for the first time mediation analyses in which we tested whether NDI, ODI, and MWF of 64 white matter fiber tracts mediated the effects of PGS_{GI} on general intelligence in a large sample of at least 500 healthy young adults. By doing so, we showed that NDI, but not ODI or MWF of white matter fiber tracts, was significantly associated with general intelligence and that the NDI of six fiber tracts mediated the relation between genes and *g*.

With regard to the three hypotheses formulated by Stammen et al. (2023) on possible links between brain characteristics and intelligence, our results provide clear evidence that differences in neurite density are crucial for differences in intelligence in the white matter, but not differences in neurite orientation dispersion or estimated myelination. Since white matter mainly consists of myelinated axons (Ocklenburg and Güntürkün 2018), this means that the number or density of axons is more important for intelligent performance than their arrangement or estimated degree of

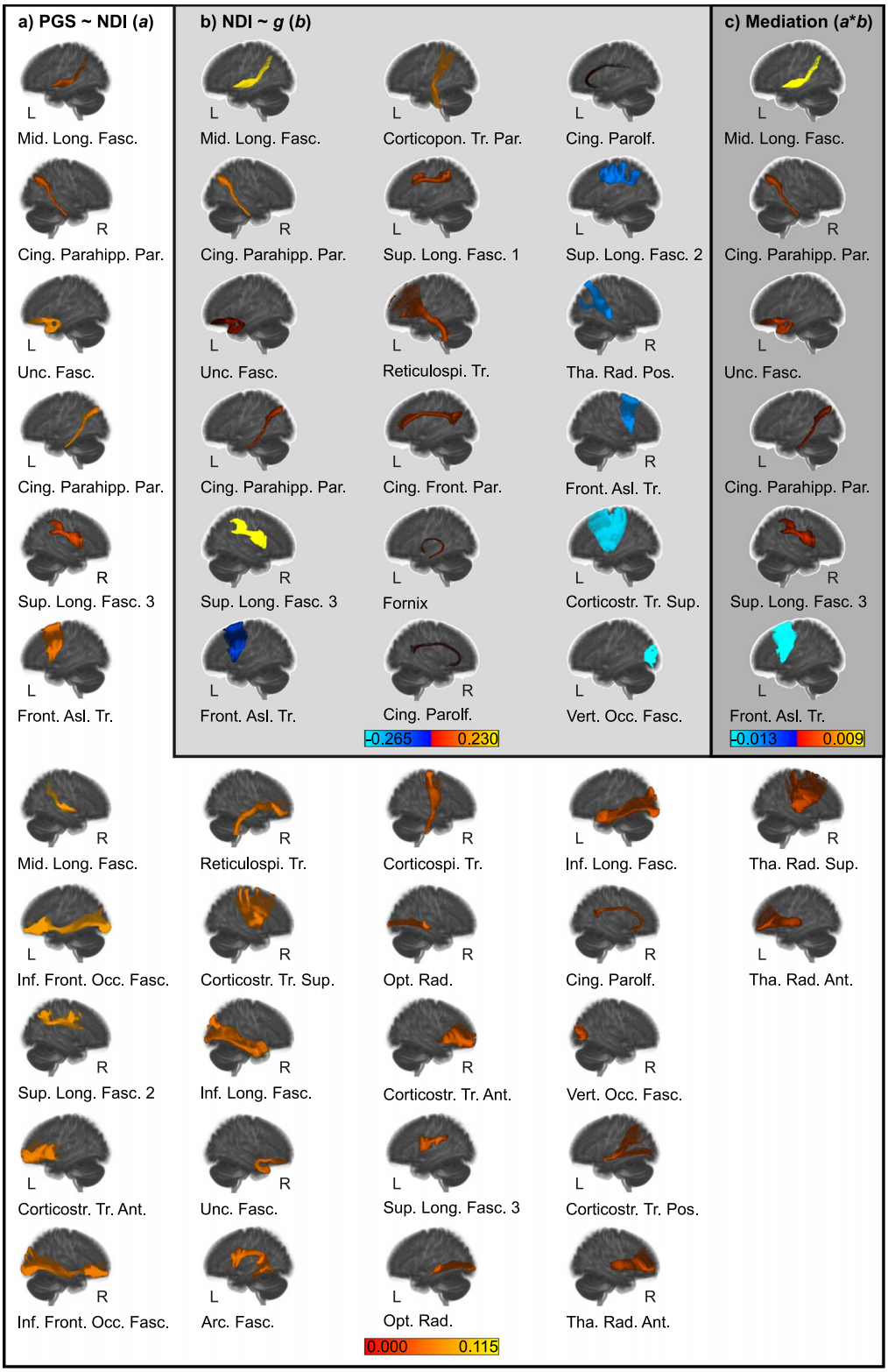

Fig. 3. Results of the multiple mediator analysis via elastic-net with neurite density index (NDI) values of 64 white matter fiber tracts as mediators after re-estimation with *lavaan*. The figure shows the results from path *a* analysis (block a) PGS ~ NDI (*a*) with white background, path *b* analysis (block b) NDI ~ *g* (*b*) with light gray background, and the mediation effects *a*∗*b* (block c) mediation (*a*∗*b*) with gray background. White matter fiber tracts are shown in left (L) or right (R) lateral view. Positive and negative effects are color-coded. For a list of white matter fiber tracts and effect sizes see Supplementary Table S1. Abbreviations: Arc. Fasc. = arcuate fasciculus; Cing. Front. Par. = cingulum frontal parietal; Cing. Parahipp. Par. = cingulum parahippocampal parietal; Cing. Parol. = cingulum parolfactory; Corticopon. Tr. Par. = corticopontine tract parietal; Corticospi. Tr. = corticospinal tract; Corticostr. Tr. Ant. = corticostriatal tract anterior; Corticostr. Tr. Pos. = corticostriatal tract posterior; Corticostr. Tr. Sup. = corticostriatal tract superior; front. Asl. Tr. = frontal aslant tract; Inf. Front. Occ. Fasc. = inferior fronto-occipital fasciculus; Inf. Long. Fasc. = inferior longitudinal fasciculus; mid. Long. Fasc. = middle longitudinal fasciculus; opt. Rad. = optic radiation; Reticulospi. Tr. = reticulospinal tract; sup. Long. Fasc. = superior longitudinal fasciculus; Tha. Rad. Ant. = thalamic radiation anterior; Tha. Rad. Pos. = thalamic radiation posterior; Tha. Rad. Sup. = thalamic radiation superior; Unc. Fasc. = uncinate fasciculus; vert. Occ. Fasc. = vertical occipital fasciculus.

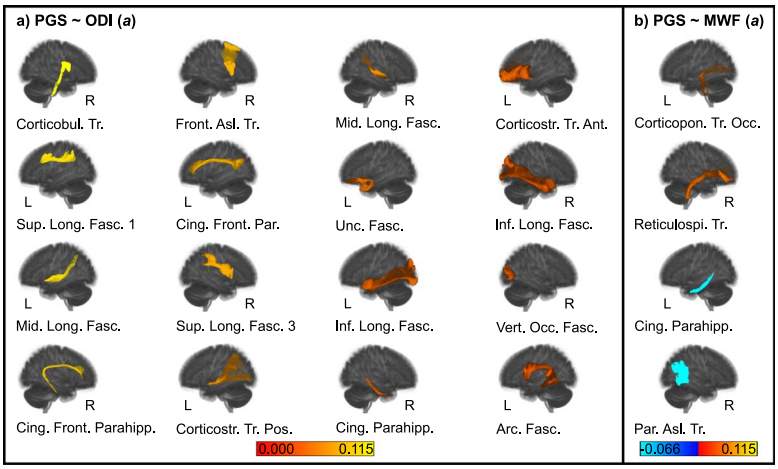

Fig. 4. Results of the multiple mediator analysis via elastic-net with neurite orientation dispersion index (ODI) values (block a) PGS ~ ODI (*a*) or myelin water fraction (MWF) values (block b) PGS ~ MWF (*a*) of 64 white matter fiber tracts as mediators after re-estimation with *lavaan*. The figure only shows the results from path *a* analyses, as no significant associations could be identified for path *b* and thus also not for paths *a*∗*b*. White matter fiber tracts are shown in left (L) or right (R) lateral view. Positive and negative effects are color-coded. For a list of white matter fiber tracts and effect sizes, see Supplementary Table S2 for ODI and Supplementary Table S3 for MWF. Abbreviations: Arc. Fasc. = arcuate fasciculus; Cing. Front. Parahipp. = cinglum frontal parahippocampal; Cing. Front. Par. = cingulum frontal parietal; Cing. Parahipp. = cingulum parahippocampal; Corticobul. Tr. = corticobulbar tract; Corticopon. Tr. Occ. = corticopontine tract occipital; Corticostr. Tr. Ant. = corticostriatal tract anterior; Corticostr. Tr. Pos. = corticostriatal tract posterior; front. Asl. Tr. = frontal aslant tract; Inf. Long. Fasc. = inferior longitudinal fasciculus; mid. Long. Fasc. = middle longitudinal fasciculus; par. Asl. Tr. = parietal aslant tract; Reticulospi. Tr. = reticulospinal tract; sup. Long. Fasc. = superior longitudinal fasciculus; Unc. Fasc. = uncinate fasciculus; vert. Occ. Fasc. = vertical occipital fasciculus.

myelination. We found that 18 white matter fiber tracts showed a significant association between NDI and intelligence. For most of the fiber tracts, the correlation was positive, which fits the hypothesized explanation of Stammen et al. (2023) that higher neurite density enables more parallel information processing by providing more possible pathways to think through problems simultaneously. It is a well-established finding that bigger brains are associated with higher levels of intelligence (McDaniel 2005; Pietschnig et al. 2015; Cox et al. 2019) and a common explanation for this phenomenon is that individuals with more cortical volume are likely to have a higher number of neurons (Pakkenberg and Gundersen 1997). Since most neurons have only a single axon (Kevenaar and Hoogenraad 2015), a higher axonal packing density suggests that there are more neurons in more intelligent individuals, which in turn provide them with enhanced computational power for problem solving and logical reasoning.

Among the white matter fiber tracts that showed a positive association between NDI and *g* were many fiber tracts whose FA values had already been associated with intelligence (Cox et al. 2019; Genç and Fraenz 2021; Stammen et al. 2023), namely, the cingulum, uncinate fasciculus, superior longitudinal fasciculus, and fornix. This means that our results complement and specify the previous FA results in terms of neurite density. All four fiber tracts have been associated with higher cognitive functions relevant to intelligence, such as attention, cognitive control, memory, visual–spatial functions, or language (Catani and Thiebaut de Schotten 2008; Benear et al. 2020; Buyanova and Arsalidou 2021). We found significant positive associations between NDI and general intelligence in bilateral parahippocampal parietal, bilateral parolfactory, and left-hemispheric frontal parietal subcomponents of the cingulum. Previous studies have shown that higher NDI in the (para) hippocampal cingulum was positively associated with higher cognition in a mixed sample of healthy older adults and patients with mild cognitive impairment or dementia (Raghavan et al. 2021), as well as with episodic memory and processing speed in healthy older adults (Gozdas et al. 2021). The analysis of Raghavan et al. (2021) also revealed that the superior longitudinal fasciculus had the strongest positive correlation between NDI and global cognition. This is consistent with our results of positive associations in the superior longitudinal fasciculus 1 in the left hemisphere and in the superior longitudinal fasciculus 3 in the right hemisphere. In contrast, our finding of an association between NDI and the left-hemispheric fornix was not found by Raghavan et al. (2021), who averaged the values of the left and right fornix for their analysis. In addition, Coad et al. (2020), who analyzed the pre- and postcommissural fornix separately, did not report any association between NDI and various cognitive factors. However, since the existing studies used different cognitive measures, defined the areas of white matter differently, and included different age groups, there are many possible factors that could have caused the different results.

Not previously noticed in FA studies on intelligence were the positive associations with the middle longitudinal fasciculus, the corticopontine tract parietal, and the reticulospinal tract in the left hemisphere. However, they were also often not included as investigated fiber tracts in previous analyses. The middle longitudinal fasciculus is an association fiber tract that connects the superior temporal gyrus with the superior parietal lobule and parietooccipital region and appears to be involved in auditory comprehension as a part of the dorsal auditory stream (Buyanova and Arsalidou 2021) and higher-order functions related to acoustic information (Latini et al. 2020). The corticopontine tract runs from the cerebral cortex through the internal capsule and ends at the unilateral pontine nucleus (Yin et al. 2023). It is part of the cerebrocerebellar system and represents an intermediate step in involving the cerebellum into the distributed neural circuits relevant to motor control, thought, and emotion (Schmahmann et al. 2019). The corticoreticulospinal tract originates from the premotor cortex, descends to the spinal cord, and is part of the extrapyramidal system (Jang and Lee 2019; Akalu et al. 2023). Although this tract is primarily associated with gross motor function, gait function, and postural stability (Jang and Lee 2019; Akalu et al. 2023), it may also be important for cognitive function in as yet unknown ways, as there is evidence that poor motor function

is associated with accelerated cognitive decline in old age (Chou et al. 2019; Wang et al. 2023).

However, there were not only tracts whose NDI was positively associated with general intelligence, but also tracts that showed a negative relation, namely, the bilateral frontal aslant tract, the left-hemispheric superior longitudinal fasciculus 2, the right-hemispheric thalamic radiation posterior, the left-hemispheric corticostriatal tract superior, and the left-hemispheric vertical occipital fasciculus. The finding that there were both positive and negative associations between white matter fiber tracts' NDI and intelligence may explain why Genç et al. (2018) as well as James et al. (2023) found no associations between cognition and total white matter NDI. Although negative associations are less straightforward to explain, we are not the first to have revealed negative associations in circumscribed areas of the brain for structural properties that are generally positively associated with intelligence (Genç et al. 2023; Williams et al. 2023). Furthermore, negative associations between neurite density of fiber tracts and specific skills such as single-word reading and phonological processing have already been reported for children (Koirala et al. 2021). At first, it seems counterintuitive that lower axonal density was associated with higher intelligence in healthy young adults as it contradicts the typical finding that "bigger is better" (McDaniel 2005; Pietschnig et al. 2015; Cox et al. 2019). However, it could be the result of the development of efficient wiring and thus signal transmission of the brain so that an optimal balance between signal and noise can be achieved and no redundant or irrelevant information is passed on, which could make efficient problem solving difficult due to inefficient circuitry (Sporns et al. 2000; Genç et al. 2018). Establishing and refining efficient brain circuits may be due to regressive events such as axon pruning or synapse elimination during neurodevelopmental processes (Riccomagno and Kolodkin 2015), which would fit well with the neural efficiency hypothesis stating that higher intelligent individuals need to invest less cortical resources while performing cognitive tasks (Haier et al. 1988; Neubauer and Fink 2009). The vertical occipital fasciculus, for example, is an association fiber tract that runs vertically at the posterolateral corner of the brain and interconnects the dorsal and ventral visual stream (Jitsuishi et al. 2020). It may be that more precise information exchange between its target regions via less dense axons is advantageous for intelligent thinking, especially since Genç et al. (2023) were able to show that lower nodal efficiency and thus more efficient wiring and signal transmission of the ventromedial visual area 1 with the rest of the brain is associated with higher intelligence. However, it remains to be seen whether future research efforts will be able to replicate our findings of negative associations between NDI of the mentioned fiber tracts and general intelligence in independent samples.

Our result that the orientation dispersion of no fiber tract was related to intelligence is consistent with the results of Callow et al. (2022), who used the ICBM-DTI-81 white matter atlas (Mori et al. 2005; Wakana et al. 2007; Hua et al. 2008) and reported a negative association in healthy adults only for the cerebellar peduncle, which was not included in our analysis. Our lack of an association at the level of individual fiber tracts is also well in line with the findings of Genç et al. (2018) and James et al. (2023), who reported no association at the global level. In contrast, Raghavan et al. (2021) showed both significant positive and negative relations between ODI and global cognition in different fiber tracts, but used a mixed sample of healthy subjects and patients for their analysis.

Although it is a long-standing hypothesis that differences in myelination may underlie differences in intelligence (Miller 1994), our results for MWF, as an estimator of myelination, showed that this is not the case for general intelligence in a sample of predominantly young adults. MWF was not significantly associated with *g* in any fiber tract of the white matter. This result is in contradiction to Penke et al. (2012), who first demonstrated an association between estimated myelination in terms of MTR and general intelligence in healthy older adults. In addition to the different estimators for myelination, the two studies differ considerably in the age of the samples examined. Interindividual differences in MWF in young adulthood may reflect a larger proportion of developmental influences and be less related to interindividual differences in general intelligence than interindividual differences in MTR in older adulthood, which may represent a larger proportion of breakdown of axonal myelination and be more related to differences in general cognitive functioning. However, Penke et al. (2012) demonstrated in their study that the association between MTR and general intelligence was completely mediated by a general factor of information processing speed. Although Page et al. (2024) showed that cerebral correlates of information processing speed and general intelligence largely overlapped, their study did not include estimators of myelination. As a result, it remains unclear whether the overlapping variance between processing speed and general intelligence—or unique portions of the variances for each cognitive variable—would exhibit strong associations with myelination. Since Penke et al. (2012) found an association between information processing speed and MTR in older adults, one possibility would be that MWF is also more specifically associated with processing speed as a more direct measure of conduction velocity and spike timing than with general intelligence. Future studies should investigate this hypothesis using samples from different age groups. Gong et al. (2023b) reported associations between lower MWF and steeper declines in processing speed in cognitively unimpaired adults and similar findings have been shown in patients with multiple sclerosis (Abel et al. 2019, 2020; Ouellette et al. 2020). Recent results also suggest correlations of indices of myelination with other cognitive abilities such as executive functions (Gong et al. 2023a) or memory performance (Mendez Colmenares et al. 2024), so that the subfactors below *g* may be more strongly influenced by differences in estimated myelination. Another way in which myelination could influence cognitive processes could be the coordination of different neuronal networks by accelerating action potentials and mediating precise timing and synchronization between neuronal ensembles (Khelfaoui et al. 2024). However, more research is needed to understand the role of myelin architecture in functional connectivity (Khelfaoui et al. 2024).

Our finding that PGS_{GI} was significantly associated with NDI of 28, ODI of 16, and MWF of four white matter fiber tracts is in accordance with previously reported results demonstrating relations between genetic variants associated with intelligence and various brain measures (Grasby et al. 2020; Lett et al. 2020; Genç et al. 2023; Williams et al. 2023). Even though few associations were found between genes for intelligence and MWF, the low proportion of fiber tracts with an association and the lack of an association between MWF and intelligence indicate that differences in intelligence may not mainly be due to differences in indices of estimated myelination, as Lee et al. (2018) had already assumed. This result also fits well with the fact that gene sets such as myelin sheath or regulation of myelination were not found to be significantly associated with intelligence in the GWAS used to calculate the PGS_{GI} (Savage et al. 2018). Although Schmitt et al. (2020), who used a different, less sensitive metric for myelination, found similar

spatial heritability patterns for indices of estimated myelination and surface area, they reported that indices of myelination, surface area, and cortical thickness were largely genetically independent in adults. Studies revealed that PGS_{GI} was associated with surface area and cortical thickness of various brain areas and that both properties of specific brain regions mediated the association between PGS_{GI} and intelligence (Lett et al. 2020; Genç et al. 2023; Williams et al. 2023). Thus, it is conceivable that genes relevant to intelligence overlap more with genes relevant to structural morphological brain properties but less with genes relevant to indices of myelination. However, it could also be that genes that overlap with intelligence and indices of myelination have not yet been found in GWAS due to small effect sizes and limited sample sizes.

Interestingly, the neurite density of six fiber tracts mediated the association between PGS_{GI} and general intelligence. Five of them, namely the left-hemispheric middle longitudinal fasciculus, the bilateral cingulum parahippocampal parietal, the left-hemispheric uncinate fasciculus, and the right-hemispheric superior longitudinal fasciculus 3, exhibited positive mediation effects, which are well in line with the results of previous mediation analyses (Lett et al. 2020; Genç et al. 2023; Williams et al. 2023). The middle longitudinal fasciculus runs from the superior temporal gyrus to the superior parietal lobule and parietooccipital region (Buyanova and Arsalidou 2021), the cingulum parahippocampal parietal from the medial temporal lobe to the parietal and occipital lobes (Wu et al. 2016), the uncinate fasciculus from the anterior temporal lobes and amygdala to the lateral orbitofrontal and anterior portion of the prefrontal cortex (Buyanova and Arsalidou 2021), and the superior longitudinal fasciculus 3 from the frontal and opercular areas to the supramarginal gyrus (Buyanova and Arsalidou 2021). Genç et al. (2023) identified the bilaterally averaged surface area of the superior medial parietal cortex, intraparietal areas, and the posterior temporal cortex as positive mediators between PGS_{GI} and intelligence and classified all of them as part of the P-FIT model (Jung and Haier 2007). Furthermore, they found the structural network efficiency of the inferior frontal gyrus to mediate positively between genes and intelligence. Lett et al. (2020) reported that the association between genetic variants and general intelligence was mediated positively by the cortical thickness and surface area of the anterior cingulate cortex, the prefrontal cortex, the insula, the medial temporal cortex, and the inferior parietal cortex. Similar mediating areas were found by Williams et al. (2023). Our results of positive mediating white matter fiber tracts thus connect regions of the brain whose morphological properties have already been identified as mediating factors between genes and intelligence and as relevant for intelligent thinking in the P-FIT model (Jung and Haier 2007). Jung and Haier (2007) assumed that the entire process of reasoning depends on the fidelity of underlying white matter and we provided evidence that a higher axonal packing density of specific white matter fiber tracts is one factor that links the genetic basis of intelligence to the corresponding phenotype.

One white matter fiber tract, namely, the left-hemispheric frontal aslant tract, had a negative mediation effect, which was due to a negative association between its NDI and general intelligence. Negative mediation effects were also reported by Genç et al. (2023), who, for example, identified the surface area of the inferior frontal sulcus as a negative mediator between genetic variants associated with educational attainment and intelligence. The frontal aslant tract runs from the pars opercularis and pars triangularis of the inferior frontal gyrus and the anterior insula to the supplementary motor area (SMA) and pre-SMA and is believed to be involved in speech planning, initiation, and production, but also kinematics and visuomotor processes (Buyanova and Arsalidou 2021). As intraoperative direct electrical stimulation of the left frontal aslant tract led to stuttering (Kemerdere et al. 2016), it could be that precise and efficient information exchange between its target regions due to lower axonal density is crucial for optimal functioning. However, the frontal aslant tract has not yet been well studied and has only recently been linked to other cognitive functions, so its role in cognition needs to be further characterized (Serrano-Sponton et al. 2024).

There are certain limitations to our study. Although elastic-net regression as a regularization method offers the advantage of handling high-dimensional and correlated data (Zou and Hastie 2005), our results should be interpreted with some caution. The procedure is inherently data driven and the selection of predictors is influenced by characteristics of the sample, correlations between predictors, or effect sizes, which means that not all relevant predictors or redundant predictors might be selected (Bunea et al. 2011). For this reason, the results should be viewed as exploratory and hypothesis generating rather than definitive, absolute, or causal. Replication in independent samples and validation using alternative analytic strategies without penalization will be important next steps to confirm the robustness and generalizability of the identified mediators. Following successful replication, a promising avenue for future research would be to investigate the hemispheric asymmetries of the selected fiber tracts in more detail, as this could provide further insight into the lateralization of intelligence-related functions. Furthermore, our paper is limited in its population representativeness as our sample mainly consisted of German university students who had a mean IQ score 1 SD above average which might have impacted the associations between genetic variants, the brain, and intelligence we observed. As neurite density as well as myelin content are associated with age (Qian et al. 2020; Buyanova and Arsalidou 2021), future studies should examine whether our results, which were limited to young adulthood, expand to other age groups or even use longitudinal designs. Furthermore, our analyses were restrained to individuals of European ancestry, thus further research is needed to investigate whether the NDI of the same white matter fiber tracts mediates the association between PGS_{GI} and general intelligence to the same degree across ancestries. As PGS_{GI} only predicted up to 5.2% of variance in general intelligence in independent samples (Savage et al. 2018), it could also be that additional white matter fiber tracts will be found when using a PGS that is based on a larger sample size and has better predictive power for intelligence. Additionally, our measures of neurite density, neurite orientation dispersion, and estimated myelination were based on neuroimaging techniques that are limited in spatial resolution. It is known that the human brain contains different classes of axons ranging from large-diameter myelinated to small-diameter unmyelinated fibers (Aboitiz et al. 1992; Liewald et al. 2014), which could not be differentiated by the methods used. Finally, we limited our study to analyzing the relation between PGS_{GI}, white matter microstructural architecture, and general intelligence in healthy subjects. However, our type of analysis can be extended to the multitude of other PGS (Cao et al. 2024), brain correlates, and phenotypes (eg intelligence subfactors) in future studies and may also provide valuable insights for clinical samples.

The present paper provides the first study examining the mediating effects of the white matter microstructural indices NDI, ODI, and MWF on the association between genetic variation and general intelligence. We showed that the neurite density of

specific white matter fiber tracts played a mediating role in the relation between cumulative genetic load for general intelligence and *g* factor performance. In contrast, we found no significant associations with general intelligence for ODI and MWF. The latter was surprising, as myelination was considered a possible neurobiological correlate of intelligence. These findings are a crucial step forward in decoding the neurogenetic underpinnings of general intelligence, as they identify that the neurite density of specific white matter fiber tracts relate polygenic variation to *g*.

Acknowledgments

The authors would like to thank Wendy Johnson for providing the *g* factor scores, all research assistants for their support during the behavioral measurements, PHILIPS Germany (Burkhard Mädler) for the scientific support with the MRI measurements as well as Tobias Otto for technical assistance.

Author contributions

Christina Stammen (Formal analysis, Investigation, Visualization, Writing—original draft, Writing—review & editing), Javier Schneider Penate (Formal analysis, Investigation, Writing—review & editing), Dorothea Metzen (Formal analysis, Writing—review & editing), Maurice J. Hönscher (Formal analysis), Christoph Fraenz (Investigation, Writing—review & editing), Caroline Schlüter (Investigation, Writing—review & editing), Onur Güntürkün (Conceptualization, Funding acquisition, Supervision, Writing—review & editing), Robert Kumsta (Conceptualization, Formal analysis, Supervision, Writing—review & editing), and Erhan Genc (Conceptualization, Formal analysis, Project administration, Resources, Supervision, Writing—original draft, Writing—review & editing). E.G., R.K., and O.G. conceived the project and supervised the experiments. E.G., C.St., R.K., and O.G. designed the project. R.K. and J.S.P. planned and performed genetic experiments. C.Sc. and C.F. collected data. C.St., E.G., J.S.P., D.M., and M.J.H. analyzed the data. C.St. and E.G. wrote the paper. All authors discussed the results and edited the manuscript.

Supplementary material

Supplementary material is available at *Cerebral Cortex* online.

Funding

This work was supported by the Deutsche Forschungsgemeinschaft (GU 227/16-1).

Conflict of interest statement: None declared.

Data availability

The data that support the findings of this study are available from the corresponding author upon reasonable request or can be downloaded from an Open Science Framework repository (https://osf.io/29cp6/).

References

Abel S et al. 2019. Myelin damage in normal appearing white matter contributes to impaired cognitive processing speed in multiple sclerosis. *J Neuroimaging*. 30:205–211. https://doi.org/10.1111/jon.12679.

Abel S et al. 2020. Associations between findings from myelin water imaging and cognitive performance among individuals with multiple sclerosis. *JAMA Netw Open*. 3:e2014220. https://doi.org/10.1001/jamanetworkopen.2020.14220.

Aboitiz F, Scheibel AB, Fisher RS, Zaidel E. 1992. Fiber composition of the human corpus callosum. *Brain Res*. 598:143–153. https://doi.org/10.1016/0006-8993(92)90178-C.

Akalu Y et al. 2023. Identifying the role of the reticulospinal tract for strength and motor recovery: a scoping review of nonhuman and human studies. *Physiol Rep*. 11:e15765 https://doi.org/10.14814/phy2.15765.

Ammerman BA et al. 2018. Exploratory analysis of mediators of the relationship between childhood maltreatment and suicidal behavior. *J Adolesc*. 69:103–112. https://doi.org/10.1016/j.adolescence.2018.09.004.

Andersson JLR, Graham MS, Zsoldos E, Sotiropoulos SN. 2016. Incorporating outlier detection and replacement into a non-parametric framework for movement and distortion correction of diffusion MR images. *Neuroimage*. 141:556–572. https://doi.org/10.1016/j.neuroimage.2016.06.058.

Andersson JLR, Jenkinson M, Smith SM. 2007. *Non-linear registration aka spatial normalisation, FMRIB technical report TR07JA2*.

Andersson JL, Skare S, Ashburner J. 2003. How to correct susceptibility distortions in spin-echo echo-planar images: application to diffusion tensor imaging. *Neuroimage*. 20:870–888. https://doi.org/10.1016/S1053-8119(03)00336-7.

Andersson JLR, Sotiropoulos SN. 2016. An integrated approach to correction for off-resonance effects and subject movement in diffusion MR imaging. *Neuroimage*. 125:1063–1078. https://doi.org/10.1016/j.neuroimage.2015.10.019.

Assaf Y, Pasternak O. 2008. Diffusion tensor imaging (DTI)-based white matter mapping in brain research: a review. *J Mol Neurosci*. 34:51–61. https://doi.org/10.1007/s12031-007-0029-0.

Baadsvik EL et al. 2023. Mapping the myelin bilayer with short-T2 MRI: methods validation and reference data for healthy human brain. *Magn Reson Med*. 89:665–677. https://doi.org/10.1002/mrm.29481.

Babyak MA. 2004. What you see may not be what you get: a brief, nontechnical introduction to overfitting in regression-type models. *Psychosom Med*. 66:411–421.

Basser PJ, Pierpaoli C. 1996. Microstructural and physiological features of tissues elucidated by quantitative-diffusion-tensor MRI. *J Magn Reson Series B*. 111:209–219. https://doi.org/10.1006/jmrb.1996.0086.

Beaulieu C. 2002. The basis of anisotropic water diffusion in the nervous system - a technical review. *NMR Biomed*. 15:435–455. https://doi.org/10.1002/nbm.782.

Benear SL, Ngo CT, Olson IR. 2020. Dissecting the fornix in basic memory processes and neuropsychiatric disease: a review. *Brain Connect*. 10:331–354. https://doi.org/10.1089/brain.2020.0749.

Bentler PM, Bonett G. 1980. Significance tests and goodness of fit in the analysis of covariance structures. *Psychol Bull*. 88:588–606. https://doi.org/10.1037/0033-2909.88.3.588.

Billiet T et al. 2015. Age-related microstructural differences quantified using myelin water imaging and advanced diffusion MRI. *Neurobiol Aging*. 36:2107–2121. https://doi.org/10.1016/j.neurobiolaging.2015.02.029.

Booth T et al. 2013. Brain white matter tract integrity and cognitive abilities in community-dwelling older people: the Lothian birth cohort, 1936. *Neuropsychol*. 27:595–607. https://doi.org/10.1037/a0033354.

Borich MR, Mackay AL, Vavasour IM, Rauscher A, Boyd LA. 2013. Evaluation of white matter myelin water fraction in chronic

stroke. *Neuroimage Clin*. 2:569–580. https://doi.org/10.1016/j.nicl.2013.04.006.

Bouhrara M et al. 2020. Adult brain aging investigated using BMC-mcDESPOT-based myelin water fraction imaging. *Neurobiol Aging*. 85:131–139. https://doi.org/10.1016/j.neurobiolaging.2019.10.003.

Bunea F et al. 2011. Penalized least squares regression methods and applications to neuroimaging. *Neuroimage*. 55:1519–1527. https://doi.org/10.1016/j.neuroimage.2010.12.028.

Buyanova IS, Arsalidou M. 2021. Cerebral white matter myelination and relations to age, gender, and cognition: a selective review. *Front Hum Neurosci*. 15:662031. https://doi.org/10.3389/fnhum.2021.662031.

Callow DD, Purcell JJ, Won J, Smith JC. 2022. Neurite dispersion and density mediates the relationship between cardiorespiratory fitness and cognition in healthy younger adults. *Neuropsychologia*. 169:108207. https://doi.org/10.1016/j.neuropsychologia.2022.108207.

Calvin CM et al. 2017. Childhood intelligence in relation to major causes of death in 68 year follow-up: prospective population study. *BMJ*. 357:j2708. https://doi.org/10.1136/bmj.j2708.

Cao C et al. 2024. PGS-depot: a comprehensive resource for polygenic scores constructed by summary statistics based methods. *Nucleic Acids Res*. 52:D963–D971. https://doi.org/10.1093/nar/gkad1029.

Catani M, Thiebaut de Schotten M. 2008. A diffusion tensor imaging tractography atlas for virtual in vivo dissections. *Cortex*. 44:1105–1132. https://doi.org/10.1016/j.cortex.2008.05.004.

Chang CC et al. 2015. Second-generation PLINK: rising to the challenge of larger and richer datasets. *Gigascience*. 4:7. https://doi.org/10.1186/s13742-015-0047-8.

Chiang MC et al. 2009. Genetics of brain fiber architecture and intellectual performance. *J Neurosci*. 29:2212–2224. https://doi.org/10.1523/JNEUROSCI.4184-08.2009.

Choi SW, Mak TS, O'Reilly PF. 2020. Tutorial: a guide to performing polygenic risk score analyses. *Nat Protoc*. 15:2759–2772. https://doi.org/10.1038/s41596-020-0353-1.

Choi SW, O'Reilly PF. 2019. PRSice-2: polygenic risk score software for biobank-scale data. *Gigascience*. 8:giz082. https://doi.org/10.1093/gigascience/giz082.

Chou MY et al. 2019. Role of gait speed and grip strength in predicting 10-year cognitive decline among community-dwelling older people. *BMC Geriatr*. 19:186. https://doi.org/10.1186/s12877-019-1199-7.

Coad BM et al. 2020. Precommissural and postcommissural fornix microstructure in healthy aging and cognition. *Brain Neurosci Adv*. 4:239821281989931–239821281989912. https://doi.org/10.1177/2398212819899316.

Cox SR, Ritchie SJ, Fawns-Ritchie C, Tucker-Drob EM, Deary IJ. 2019. Structural brain imaging correlates of general intelligence in UK biobank. *Intelligence*. 76:101376. https://doi.org/10.1016/j.intell.2019.101376.

Cox SR et al. 2016. Ageing and brain white matter structure in 3,513 UK Biobank participants. *Nat Commun*. 7:13629. https://doi.org/10.1038/ncomms13629.

Cremers LG et al. 2016. Altered tract-specific white matter microstructure is related to poorer cognitive performance: the Rotterdam study. *Neurobiol Aging*. 39:108–117. https://doi.org/10.1016/j.neurobiolaging.2015.11.021.

Daducci A et al. 2015. Accelerated microstructure imaging via convex optimization (AMICO) from diffusion MRI data. *Neuroimage*. 105:32–44. https://doi.org/10.1016/j.neuroimage.2014.10.026.

Das S et al. 2016. Next-generation genotype imputation service and methods. *Nat Genet*. 48:1284–1287. https://doi.org/10.1038/ng.3656.

Davies G et al. 2018. Study of 300,486 individuals identifies 148 independent genetic loci influencing general cognitive function. *Nat Commun*. 9:2098. https://doi.org/10.1038/s41467-018-04362-x.

Deary IJ. 2014. The stability of intelligence from childhood to old age. *Curr Dir Psychol Sci*. 23:239–245. https://doi.org/10.1177/0963721414536905.

Deary IJ, Cox SR, Hill WD. 2022. Genetic variation, brain, and intelligence differences. *Mol Psychiatry*. 27:335–353. https://doi.org/10.1038/s41380-021-01027-y.

Dunst B, Benedek M, Koschutnig K, Jauk E, Neubauer AC. 2014. Sex differences in the IQ-white matter microstructure relationship: a DTI study. *Brain Cogn*. 91:71–78. https://doi.org/10.1016/j.bandc.2014.08.006.

Dvorak AV et al. 2021. An atlas for human brain myelin content throughout the adult life span. *Sci Rep*. 11:269. https://doi.org/10.1038/s41598-020-79540-3.

Elliott ML et al. 2019. A polygenic score for higher educational attainment is associated with larger brains. *Cereb Cortex*. 29:3496–3504. https://doi.org/10.1093/cercor/bhy219.

Erdodi LA et al. 2017. Wechsler Adult Intelligence Scale-Fourth Edition (WAIS-IV) processing speed scores as measures of noncredible responding: the third generation of embedded performance validity indicators. *Psychol Assess*. 29:148–157. https://doi.org/10.1037/pas0000319.

Fan CC et al. 2022. Multivariate genome-wide association study on tissue-sensitive diffusion metrics highlights pathways that shape the human brain. *Nat Commun*. 13:2423. https://doi.org/10.1038/s41467-022-30110-3.

Faulkner ME et al. 2024. Harnessing myelin water fraction as an imaging biomarker of human cerebral aging, neurodegenerative diseases, and risk factors influencing myelination: a review. *J Neurochem*. 168:2243–2263. https://doi.org/10.1111/jnc.16170.

Flanagan DP, Dixon SG. 2013. The Cattell-Horn-Carroll theory of cognitive abilities. In: *Encyclopedia of special education* Reynolds CR, Vannest KJ, Fletcher-Janzen E (eds). John Wiley & Sons, Hoboken, New Jersey.

Fonov V et al. 2011. Unbiased average age-appropriate atlases for pediatric studies. *Neuroimage*. 54:313–327. https://doi.org/10.1016/j.neuroimage.2010.07.033.

Fraenz C et al. 2021. Interindividual differences in matrix reasoning are linked to functional connectivity between brain regions nominated by parieto-frontal integration theory. *Intelligence*. 87:101545. https://doi.org/10.1016/j.intell.2021.101545.

Friedrich P et al. 2020. The relationship between axon density, myelination, and fractional anisotropy in the human corpus callosum. *Cereb Cortex*. 30:2042–2056. https://doi.org/10.1093/cercor/bhz221.

Froeling M, Tax CMW, Vos SB, Luijten PR, Leemans A. 2017. "MASSIVE" brain dataset: multiple acquisitions for standardization of structural imaging validation and evaluation. *Magn Reson Med*. 77:1797–1809. https://doi.org/10.1002/mrm.26259.

Gareau PJ, Rutt BK, Karlik SJ, Mitchell JR. 2000. Magnetization transfer and multicomponent T2 relaxation measurements with histopathologic correlation in an experimental model of MS. *J Magn Reson Imaging*. 11:586–595. https://doi.org/10.1002/1522-2586(200006)11:6<586::AID-JMRI3>3.0.CO;2-V.

Genç E, Fraenz C. 2021. Diffusion-weighted imaging of intelligence. In: Barbey AK, Karama S, Haier RJ, editors. *The Cambridge handbook of intelligence and cognitive neuroscience*. Cambridge University Press, Cambridge, United Kingdom, p. 191–209 https://doi.org/10.1017/9781108635462.014.

Genç E et al. 2018. Diffusion markers of dendritic density and arborization in gray matter predict differences in intelligence. *Nat Commun*. 9:1905. https://doi.org/10.1038/s41467-018-04268-8.

Genç E et al. 2019. The neural architecture of general knowledge. *EJP*. 33:589–605. https://doi.org/10.1002/per.2217.

Genç E et al. 2021. Polygenic scores for cognitive abilities and their association with different aspects of general intelligence—a deep phenotyping approach. *Mol Neurobiol*. 58:4145–4156. https://doi.org/10.1007/s12035-021-02398-7.

Genç E et al. 2023. Structural architecture and brain network efficiency link polygenic scores to intelligence. *Hum Brain Mapp*. 44: 3359–3376. https://doi.org/10.1002/hbm.26286.

Gong Z, Bilgel M, Resnick SM, An Y, Bouhrara M. 2023a. White matter myelination is associated with longitudinal changes in processing speed in normative aging. *Alzheimers Dement*. 19:e076956. https://doi.org/10.1002/alz.076956.

Gong Z et al. 2023b. Lower myelin content is associated with more rapid cognitive decline among cognitively unimpaired individuals. *Alzheimers Dement*. 19:3098–3107. https://doi.org/10.1002/alz.12968.

Góngora D, Vega-Hernández M, Jahanshahi M, Valdés-Sosa PA, Bringas-Vega ML. 2020. Crystallized and fluid intelligence are predicted by microstructure of specific white-matter tracts. *Hum Brain Mapp*. 41:906–916. https://doi.org/10.1002/hbm.24848.

Gozdas E, Fingerhut H, Dacorro L, Bruno JL, Hosseini SMH. 2021. Neurite imaging reveals widespread alterations in gray and white matter neurite morphology in healthy aging and amnestic mild cognitive impairment. *Cereb Cortex*. 31:5570–5578. https://doi.org/10.1093/cercor/bhab180.

Grasby KL et al. 2020. The genetic architecture of the human cerebral cortex. *Science*. 367:eaay6690. https://doi.org/10.1126/science.aay6690.

Greve DN, Fischl B. 2009. Accurate and robust brain image alignment using boundary-based registration. *Neuroimage*. 48:63–72. https://doi.org/10.1016/j.neuroimage.2009.06.060.

Grussu F et al. 2017. Neurite dispersion: a new marker of multiple sclerosis spinal cord pathology? *Ann Clin Transl Neurol*. 4:663–679. https://doi.org/10.1002/acn3.445.

Haier RJ et al. 1988. Cortical glucose metabolic rate correlates of abstract reasoning and attention studied with positron emission tomography. *Intelligence*. 12:199–217. https://doi.org/10.1016/0160-2896(88)90016-5.

Harms RL, Fritz FJ, Tobisch A, Goebel R, Roebroeck A. 2017. Robust and fast nonlinear optimization of diffusion MRI microstructure models. *Neuroimage*. 155:82–96. https://doi.org/10.1016/j.neuroimage.2017.04.064.

Harms RL, Roebroeck A. 2018. Robust and fast Markov chain Monte Carlo sampling of diffusion MRI microstructure models. *Front Neuroinform*. 12:97. https://doi.org/10.3389/fninf.2018.00097.

Haworth CM et al. 2010. The heritability of general cognitive ability increases linearly from childhood to young adulthood. *Mol Psychiatry*. 15:1112–1120. https://doi.org/10.1038/mp.2009.55.

Hennig J. 1988. Multiecho imaging sequences with low refocusing flip angles. *J Magn Reson*. 78:397–407. https://doi.org/10.1016/0022-2364(88)90128-X.

Hennig J, Weigel M, Scheffler K. 2003. Multiecho sequences with variable refocusing flip angles: optimization of signal behavior using smooth transitions between pseudo steady states (TRAPS). *Magn Reson Med*. 49:527–535. https://doi.org/10.1002/mrm.10391.

Herlin B, Uszynski I, Chauvel M, Dupont S, Poupon C. 2024. Sex-related variability of white matter tracts in the whole HCP cohort. *Brain Struct Funct*. 229:1713–1735. https://doi.org/10.1007/s00429-024-02833-0.

Hidese S et al. 2020. Correlation between the Wechsler Adult Intelligence Scale- 3rd edition metrics and brain structure in healthy individuals: a whole-brain magnetic resonance imaging study. *Front Hum Neurosci*. 14:211. https://doi.org/10.3389/fnhum.2020.00211.

Hill WD et al. 2019. A combined analysis of genetically correlated traits identifies 187 loci and a role for neurogenesis and myelination in intelligence. *Mol Psychiatry*. 24:169–181. https://doi.org/10.1038/s41380-017-0001-5.

Hoerl AR, Kennard RW. 2000. Ridge regression: biased estimation for nonorthogonal problems. *Technometrics*. 12:80–86.

Holleran L et al. 2020. The relationship between white matter microstructure and general cognitive ability in patients with schizophrenia and healthy participants in the ENIGMA consortium. *Am J Psychiatry*. 177:537–547. https://doi.org/10.1176/appi.ajp.2019.19030225.

Hossiep R, Hasella M, Turck D. 2001. *BOMAT-advanced-short version: Bochumer Matrizentest*. Hogrefe, Göttingen (Germany).

Hossiep R, Schulte M. 2008. *BOWIT: Bochumer Wissenstest*. Hogrefe, Göttingen (Germany).

Hu L, Bentler PM. 1999. Cutoff criteria for fit indexes in covariance structure analysis: conventional criteria versus new alternatives. *Struct Equ Model*. 6:1–55. https://doi.org/10.1080/10705519909540118.

Hua K et al. 2008. Tract probability maps in stereotaxic spaces: analyses of white matter anatomy and tract-specific quantification. *Neuroimage*. 39:336–347. https://doi.org/10.1016/j.neuroimage.2007.07.053.

Hunt BA et al. 2016. Relationships between cortical myeloarchitecture and electrophysiological networks. *Proc Natl Acad Sci USA*. 113:13510–13515. https://doi.org/10.1073/pnas.1608587113.

Jacobucci R et al. 2022. *Regsem: Regularized Structural Equation Modeling*. R package version 1.9.3. https://CRAN.Rproject.org/package=regsem.

Jaeggi SM, Buschkuehl M, Jonides J, Perrig WJ. 2008. Improving fluid intelligence with training on working memory. *Proc Natl Acad Sci USA*. 105:6829–6833. https://doi.org/10.1073/pnas.0801268105.

James SN et al. 2023. Neuroimaging, clinical and life course correlates of normal-appearing white matter integrity in 70-year-olds. *Brain Commun*. 5:fcad225. https://doi.org/10.1093/braincomms/fcad225.

Jang SH, Lee SJ. 2019. Corticoreticular tract in the human brain: a mini review. *Front Neurol*. 10:1188. https://doi.org/10.3389/fneur.2019.01188.

Jenkinson M, Bannister P, Brady M, Smith S. 2002. Improved optimization for the robust and accurate linear registration and motion correction of brain images. *Neuroimage*. 17:825–841. https://doi.org/10.1006/nimg.2002.1132.

Jenkinson M, Smith SM. 2001. A global optimisation method for robust affine registration of brain images. *Med Image Anal*. 5: 143–156. https://doi.org/10.1016/S1361-8415(01)00036-6.

Jespersen SN, Leigland LA, Cornea A, Kroenke CD. 2012. Determination of axonal and dendritic orientation distributions within the developing cerebral cortex by diffusion tensor imaging. *IEEE Trans Med Imaging*. 31:16–32. https://doi.org/10.1109/TMI.2011.2162099.

Jespersen SN et al. 2010. Neurite density from magnetic resonance diffusion measurements at ultrahigh field: comparison with light microscopy and electron microscopy. *Neuroimage*. 49:205–216. https://doi.org/10.1016/j.neuroimage.2009.08.053.

Jitsuishi T et al. 2020. White matter dissection and structural connectivity of the human vertical occipital fasciculus to link vision-associated brain cortex. *Sci Rep*. 10:820. https://doi.org/10.1038/s41598-020-57837-7.

Johnson W, Bouchard TJ, Krueger RF, McGue M, Gottesman II. 2004. Just one g: consistent results from three test batteries. *Intelligence*. 32:95–107. https://doi.org/10.1016/S0160-2896(03)00062-X.

Johnson W, te Nijenhuis J, Bouchard TJ. 2008. Still just 1 g: consistent results from five test batteries. *Intelligence*. 36:81–95. https://doi.org/10.1016/j.intell.2007.06.001.

Jones DK, Knösche TR, Turner R. 2013. White matter integrity, fiber count, and other fallacies: the do's and don'ts of diffusion MRI. *Neuroimage*. 73:239–254. https://doi.org/10.1016/j.neuroimage.2012.06.081.

Jöreskog KG. 1969. A general approach to confirmatory maximum likelihood factor analysis. *Psychometrika*. 34:183–202. https://doi.org/10.1007/BF02289343.

Jung RE, Haier RJ. 2007. The parieto-frontal integration theory (P-FIT) of intelligence: converging neuroimaging evidence. *Behav Brain Sci*. 30:135–154. https://doi.org/10.1017/S0140525X07001185.

Kemerdere R et al. 2016. Role of the left frontal aslant tract in stuttering: a brain stimulation and tractographic study. *J Neurol*. 263:157–167. https://doi.org/10.1007/s00415-015-7949-3.

Kevenaar JT, Hoogenraad CC. 2015. The axonal cytoskeleton: from organization to function. *Front Mol Neurosci*. 8:44. https://doi.org/10.3389/fnmol.2015.00044.

Khelfaoui H, Ibaceta-Gonzalez C, Angulo MC. 2024. Functional myelin in cognition and neurodevelopmental disorders. *Cell Mol Life Sci*. 81:181. https://doi.org/10.1007/s00018-024-05222-2.

Kievit RA, Fuhrmann D, Borgeest GS, Simpson-Kent IL, Henson RNA. 2018. The neural determinants of age-related changes in fluid intelligence: a pre-registered, longitudinal analysis in UK Biobank. *Wellcome Open Res*. 3:38 https://doi.org/http://dx.doi.org/10.12688/wellcomeopenres.14241.2.

Kievit RA et al. 2014. Distinct aspects of frontal lobe structure mediate age-related differences in fluid intelligence and multitasking. *Nat Commun*. 5:5658. https://doi.org/10.1038/ncomms6658.

Kievit RA et al. 2016. A watershed model of individual differences in fluid intelligence. *Neuropsychologia*. 91:186–198. https://doi.org/10.1016/j.neuropsychologia.2016.08.008.

Kodiweera C, Alexander AL, Harezlak J, McAllister TW, Wu YC. 2016. Age effects and sex differences in human brain white matter of young to middle-aged adults: a DTI, NODDI, and q-space study. *Neuroimage*. 128:180–192. https://doi.org/10.1016/j.neuroimage.2015.12.033.

Koirala N, Perdue MV, Su X, Grigorenko EL, Landi N. 2021. Neurite density and arborization is associated with reading skill and phonological processing in children. *Neuroimage*. 241:118426. https://doi.org/10.1016/j.neuroimage.2021.118426.

Latini F et al. 2020. New insights into the anatomy, connectivity and clinical implications of the middle longitudinal fasciculus. *Front Neuroanat*. 14:610324.

Laule C et al. 2006. Myelin water imaging in multiple sclerosis: quantitative correlations with histopathology. *Mult Scler*. 12:747–753. https://doi.org/10.1177/1352458506070928.

Laule C et al. 2007. Magnetic resonance imaging of myelin. *Neurotherapeutics*. 4:460–484. https://doi.org/10.1016/j.nurt.2007.05.004.

Laule C et al. 2008. Myelin water imaging of multiple sclerosis at 7 T: correlations with histopathology. *Neuroimage*. 40:1575–1580. https://doi.org/10.1016/j.neuroimage.2007.12.008.

Laule C et al. 2016. High-resolution myelin water imaging in postmortem multiple sclerosis spinal cord: a case report. *Mult Scler*. 22:1485–1489. https://doi.org/10.1177/1352458515624559.

Lawrence KE et al. 2021. Age and sex effects on advanced white matter microstructure measures in 15,628 older adults: a UK Biobank study. *Brain Imaging Behav*. 15:2813–2823. https://doi.org/10.1007/s11682-021-00548-y.

Le Bihan D. 2003. Looking into the functional architecture of the brain with diffusion MRI. *Nat Rev Neurosci*. 4:469–480. https://doi.org/10.1038/nrn1119.

Lee JJ et al. 2018. Gene discovery and polygenic prediction from a genome-wide association study of educational attainment in 1.1 million individuals. *Nat Genet*. 50:1112–1121. https://doi.org/10.1038/s41588-018-0147-3.

Leemans A, Jeurissen B, Sijbers J, Jones DK. 2009. ExploreDTI: a graphical toolbox for processing, analyzing, and visualizing diffusion MR data. *Proc Intl Soc Mag Reson Med*. 17:3537.

Lett TA et al. 2020. Cortical surfaces mediate the relationship between polygenic scores for intelligence and general intelligence. *Cereb Cortex*. 30:2707–2718. https://doi.org/10.1093/cercor/bhz270.

Liepmann D, Beauducel A, Brocke B, Amthauer R. 2007. *Intelligenz-Struktur-test 2000 R (I-S-T 2000 R). Manual*. Hogrefe, Göttingen (Germany).

Liewald D, Miller R, Logothetis N, Wagner HJ, Schuz A. 2014. Distribution of axon diameters in cortical white matter: an electron-microscopic study on three human brains and a macaque. *Biol Cybern*. 108:541–557. https://doi.org/10.1007/s00422-014-0626-2.

MacKay AL, Laule C. 2016. Magnetic resonance of myelin water: an in vivo marker for myelin. *Brain Plast*. 2:71–91. https://doi.org/10.3233/BPL-160033.

Malpas CB et al. 2016. MRI correlates of general intelligence in neurotypical adults. *J Clin Neurosci*. 24:128–134. https://doi.org/10.1016/j.jocn.2015.07.012.

McDaniel M. 2005. Big-brained people are smarter: a meta-analysis of the relationship between in vivo brain volume and intelligence. *Intelligence*. 33:337–346. https://doi.org/10.1016/j.intell.2004.11.005.

McNeish DM. 2015. Using lasso for predictor selection and to assuage overfitting: a method long overlooked in behavioral sciences. *Multivariate Behav Res*. 50:471–484. https://doi.org/10.1080/00273171.2015.1036965.

Meinert S et al. 2022. Association of brain white matter microstructure with cognitive performance in major depressive disorder and healthy controls: a diffusion-tensor imaging study. *Mol Psychiatry*. 27:1103–1110. https://doi.org/10.1038/s41380-021-01330-8.

Mendez Colmenares A et al. 2024. Testing the structural disconnection hypothesis: myelin content correlates with memory in healthy aging. *Neurobiol Aging*. 141:21–33. https://doi.org/10.1016/j.neurobiolaging.2024.05.013.

Meyers SM et al. 2013. Multicenter measurements of myelin water fraction and geometric mean T2: intra- and intersite reproducibility. *J Magn Reson Imaging*. 38:1445–1453. https://doi.org/10.1002/jmri.24106.

Miller EM. 1994. Intelligence and brain myelination: a hypothesis. *Pers Individ Differ*. 17:803–832. https://doi.org/10.1016/0191-8869(94)90049-3.

Mitchell BL et al. 2020. Educational attainment polygenic scores are associated with cortical total surface area and regions important for language and memory. *Neuroimage*. 212:116691. https://doi.org/10.1016/j.neuroimage.2020.116691.

Mori S, Wakana S, van Zijl PCM, Nagae-Poetscher LM. 2005. *MRI atlas of human white matter*. Elsevier B. V.

Nave KA. 2010. Myelination and support of axonal integrity by glia. *Nature*. 468:244–252. https://doi.org/10.1038/nature09614.

Neisser U et al. 1996. Intelligence: knowns and unknowns. *Am Psychol*. 51:77–101. https://doi.org/10.1037/0003-066X.51.2.77.

Neubauer AC, Fink A. 2009. Intelligence and neural efficiency. *Neurosci Biobehav Rev*. 33:1004–1023. https://doi.org/10.1016/j.neubiorev.2009.04.001.

Ocklenburg S, Güntürkün O. 2018. *Structural hemispheric asymmetries. The lateralized brain: the neuroscience and evolution of hemispheric asymmetries*. London (United Kingdom): Academic Press. p. 239–262. https://doi.org/10.1016/B978-0-12-803452-1.00009-6.

Ocklenburg S et al. 2019. Myelin water fraction imaging reveals hemispheric asymmetries in human white matter that are associated with genetic variation in PLP1. *Mol Neurobiol*. 56:3999–4012. https://doi.org/10.1007/s12035-018-1351-y.

Oelhafen S et al. 2013. Increased parietal activity after training of interference control. *Neuropsychologia*. 51:2781–2790. https://doi.org/10.1016/j.neuropsychologia.2013.08.012.

Oldfield RC. 1971. The assessment and analysis of handedness: the Edinburgh inventory. *Neuropsychologia*. 9:97–113. https://doi.org/10.1016/0028-3932(71)90067-4.

Oswald WD, Roth E. 1987. *Der Zahlen-Verbindungs-test (ZVT)*. Hogrefe, Göttingen (Germany).

Ouellette R et al. 2020. Validation of rapid magnetic resonance myelin imaging in multiple sclerosis. *Ann Neurol*. 87:710–724. https://doi.org/10.1002/ana.25705.

Page D et al. 2024. Examining the neurostructural architecture of intelligence: The Lothian Birth Cohort 1936 study. *Cortex*. 178: 269–286. https://doi.org/10.1016/j.cortex.2024.06.007.

Pakkenberg B, Gundersen HJ. 1997. Neocortical neuron number in humans: effect of sex and age. *J Comp Neurol*. 384:312–320. https://doi.org/10.1002/(SICI)1096-9861(19970728)384:2<312::AID-CNE10>3.0.CO;2-K.

Penke L et al. 2010. A general factor of brain white matter integrity predicts information processing speed in healthy older people. *J Neurosci*. 30:7569–7574. https://doi.org/10.1523/JNEUROSCI.1553-10.2010.

Penke L et al. 2012. Brain white matter tract integrity as a neural foundation for general intelligence. *Mol Psychiatry*. 17:1026–1030. https://doi.org/10.1038/mp.2012.66.

Pietschnig J, Penke L, Wicherts JM, Zeiler M, Voracek M. 2015. Meta-analysis of associations between human brain volume and intelligence differences: how strong are they and what do they mean? *Neurosci Biobehav Rev*. 57:411–432. https://doi.org/10.1016/j.neubiorev.2015.09.017.

Plomin R, von Stumm S. 2018. The new genetics of intelligence. *Nat Rev Genet*. 19:148–159. https://doi.org/10.1038/nrg.2017.104.

Polderman TJ et al. 2015. Meta-analysis of the heritability of human traits based on fifty years of twin studies. *Nat Genet*. 47:702–709. https://doi.org/10.1038/ng.3285.

Powell MJD. 1964. An efficient method for finding the minimum of a function of several variables without calculating derivatives. *Comput J*. 7:155–162. https://doi.org/10.1093/comjnl/7.2.155.

Prasloski T et al. 2012. Rapid whole cerebrum myelin water imaging using a 3D GRASE sequence. *Neuroimage*. 63:533–539. https://doi.org/10.1016/j.neuroimage.2012.06.064.

Price AL et al. 2006. Principal components analysis corrects for stratification in genome-wide association studies. *Nat Genet*. 38: 904–909. https://doi.org/https://doi.org/10.1038/ng1847.

Purcell S, Chang C. PLINK 1.9 [Internet]. www.cog-genomics.org/plink/1.9/.

Qian W, Khattar N, Cortina LE, Spencer RG, Bouhrara M. 2020. Nonlinear associations of neurite density and myelin content with age revealed using multicomponent diffusion and relaxometry magnetic resonance imaging. *Neuroimage*. 223:117369. https://doi.org/10.1016/j.neuroimage.2020.117369.

R Core Team. 2022. *R: a language and environment for statistical computing*, 4.2.2 edn. R Foundation for Statistical Computing, Vienna, Austria.

Raghavan S et al. 2021. Diffusion models reveal white matter microstructural changes with ageing, pathology and cognition. *Brain Commun*. 3:fcab106. https://doi.org/10.1093/braincomms/fcab106.

Raven JC, Court JH, Raven J. 1990. *Coloured progressive matrices. Manual for Raven's progressive matrices and vocabulary scales*. Oxford Psychologists Press, Oxford (United Kingdom).

Riccomagno MM, Kolodkin AL. 2015. Sculpting neural circuits by axon and dendrite pruning. *Annu Rev Cell Dev Biol*. 31:779–805. https://doi.org/10.1146/annurev-cellbio-100913-013038.

Rosseel Y. 2012. Lavaan: an R package for structural equation modeling. *J Stat Softw*. 48:1–36 http://dx.doi.org/10.18637/jss.v048.i02.

Roth B et al. 2015. Intelligence and school grades: a meta-analysis. *Intelligence*. 53:118–137. https://doi.org/10.1016/j.intell.2015.09.002.

RStudio Team. 2022. *RStudio: integrated development environment for R*, 2022.12.0.353 edn. Posit Software, PBC, Boston, MA.

Savage JE et al. 2018. Genome-wide association meta-analysis in 269,867 individuals identifies new genetic and functional links to intelligence. *Nat Genet*. 50:912–919. https://doi.org/10.1038/s41588-018-0152-6.

Schlüter C, Fraenz C, Friedrich P, Güntürkün O, Genç E. 2022. Neurite density imaging in amygdala nuclei reveals interindividual differences in neuroticism. *Hum Brain Mapp*. 43:2051–2063. https://doi.org/10.1002/hbm.25775.

Schmahmann JD, Guell X, Stoodley CJ, Halko MA. 2019. The theory and neuroscience of cerebellar cognition. *Annu Rev Neurosci*. 42: 337–364. https://doi.org/10.1146/annurev-neuro-070918-050258.

Schmidt FL, Hunter J. 2004. General mental ability in the world of work: occupational attainment and job performance. *J Pers Soc Psychol*. 86:162–173. https://doi.org/10.1037/0022-3514.86.1.162.

Schmitt JE, Raznahan A, Liu S, Neale MC. 2020. The genetics of cortical myelination in young adults and its relationships to cerebral surface area, cortical thickness, and intelligence: a magnetic resonance imaging study of twins and families. *Neuroimage*. 206:116319. https://doi.org/10.1016/j.neuroimage.2019.116319.

Schneider WJ, McGrew KS. 2012. The Cattell-Horn-Carroll model of intelligence. In: *Contemporary intellectual assessment: theories, tests, and issues* Flanagan DP, Harrison PL (eds), 3rd edn. Guilford Press, New York, p. 99–144.

Serang S, Jacobucci R. 2020. Exploratory mediation analysis of dichotomous outcomes via regularization. *Multivariate Behav Res*. 55:69–86. https://doi.org/10.1080/00273171.2019.1608145.

Serang S, Jacobucci R, Brimhall KC, Grimm KJ. 2017. Exploratory mediation analysis via regularization. *Struct Equ Modeling*. 24: 733–744. https://doi.org/10.1080/10705511.2017.1311775.

Serrano-Sponton L et al. 2024. Harnessing the frontal aslant tract's structure to assess its involvement in cognitive functions: new insights from 7-T diffusion imaging. *Sci Rep*. 14:17455. https://doi.org/10.1038/s41598-024-67013-w.

Smith SM et al. 2004. Advances in functional and structural MR image analysis and implementation as FSL. *Neuroimage*. 23: S208–S219. https://doi.org/10.1016/j.neuroimage.2004.07.051.

Spearman C. 1904. "General intelligence," objectively determined and measured. *Am J Psychol*. 15:201–292. https://doi.org/10.2307/1412107.

Sporns O, Tononi G, Edelman GM. 2000. Connectivity and complexity: the relationship between neuroanatomy and brain dynamics. *Neural Netw*. 13:909–922. https://doi.org/10.1016/S0893-6080(00)00053-8.

Stammen C et al. 2023. Robust associations between white matter microstructure and general intelligence. *Cereb Cortex*. 33: 6723–6741. https://doi.org/10.1093/cercor/bhac538.

Strenze T. 2007. Intelligence and socioeconomic success: a meta-analytic review of longitudinal research. *Intelligence*. 35:401–426. https://doi.org/10.1016/j.intell.2006.09.004.

Tamnes CK et al. 2010. Intellectual abilities and white matter microstructure in development: a diffusion tensor imaging study. *Hum Brain Mapp.* 31:1609–1625. https://doi.org/10.1002/hbm.20962.

Tang CY et al. 2010. Brain networks for working memory and factors of intelligence assessed in males and females with fMRI and DTI. *Intelligence.* 38:293–303. https://doi.org/10.1016/j.intell.2010.03.003.

Tian Y, Zhang Y. 2022. A comprehensive survey on regularization strategies in machine learning. *Inf Fusion.* 80:146–166. https://doi.org/10.1016/j.inffus.2021.11.005.

Tibshirani R. 1996. Regression shrinkage and selection via the lasso. *J R Statist Soc B.* 58:267–288. https://doi.org/10.1111/j.2517-6161.1996.tb02080.x.

Van Essen DC et al. 2013. The WU-Minn human connectome project: an overview. *Neuroimage.* 80:62–79. https://doi.org/10.1016/j.neuroimage.2013.05.041.

Vargas WS et al. 2015. Measuring longitudinal myelin water fraction in new multiple sclerosis lesions. *Neuroimage Clin.* 9:369–375. https://doi.org/10.1016/j.nicl.2015.09.003.

Vavasour IM, Clark CM, Li DK, Mackay AL. 2006. Reproducibility and reliability of MR measurements in white matter: clinical implications. *Neuroimage.* 32:637–642. https://doi.org/10.1016/j.neuroimage.2006.03.036.

Vavasour IM, Laule C, Li DK, Traboulsee AL, MacKay AL. 2011. Is the magnetization transfer ratio a marker for myelin in multiple sclerosis? *J Magn Reson Imaging.* 33:713–718. https://doi.org/10.1002/jmri.22441.

Vos SB et al. 2017. The importance of correcting for signal drift in diffusion MRI. *Magn Reson Med.* 77:285–299. https://doi.org/10.1002/mrm.26124.

Wakana S et al. 2007. Reproducibility of quantitative tractography methods applied to cerebral white matter. *Neuroimage.* 36:630–644. https://doi.org/10.1016/j.neuroimage.2007.02.049.

Wang Z et al. 2023. Association of motor function with cognitive trajectories and structural brain differences: a community-based cohort study. *Neurol.* 101:e1718–e1728. https://doi.org/10.1212/WNL.0000000000207745.

Whittal KP, MacKay AL. 1989. Quantitative interpretation of NMR relaxation data. *J Magn Reson.* 84:134–152.

Whittall KP et al. 1997. In vivo measurement of T2 distributions and water contents in normal human brain. *Magn Reson Med.* 37:34–43. https://doi.org/10.1002/mrm.1910370107.

Wilcox RR. 1997. *Introduction to robust estimation and hypothesis testing*. Academic Press, San Diego.

Williams CM, Peyre H, Ramus F. 2023. Brain volumes, thicknesses, and surface areas as mediators of genetic factors and childhood adversity on intelligence. *Cereb Cortex.* 33:5885–5895. https://doi.org/10.1093/cercor/bhac468.

Wu Y, Sun D, Wang Y, Wang Y, Ou S. 2016. Segmentation of the cingulum bundle in the human brain: a new perspective based on DSI tractography and fiber dissection study. *Front Neuroanat.* 10:84. https://doi.org/10.3389/fnana.2016.00084.

Yeh FC. 2022. Population-based tract-to-region connectome of the human brain and its hierarchical topology. *Nat Commun.* 13:4933. https://doi.org/10.1038/s41467-022-32595-4.

Yeh FC et al. 2018. Population-averaged atlas of the macroscale human structural connectome and its network topology. *Neuroimage.* 178:57–68. https://doi.org/10.1016/j.neuroimage.2018.05.027.

Yeung HW et al. 2023. Predicting sex, age, general cognition and mental health with machine learning on brain structural connectomes. *Hum Brain Mapp.* 44:1913–1933. https://doi.org/10.1002/hbm.26182.

Yin H et al. 2023. The language-related cerebro-cerebellar pathway in humans: a diffusion imaging-based tractographic study. *Quant Imaging Med Surg.* 13:1399–1416 https://doi.org/http://dx.doi.org/10.21037/qims-22-303.

Zagorsky JL. 2007. Do you have to be smart to be rich? The impact of IQ on wealth, income and financial distress. *Intelligence.* 35:489–501. https://doi.org/10.1016/j.intell.2007.02.003.

Zhang H, Schneider T, Wheeler-Kingshott CA, Alexander DC. 2012. NODDI: practical in vivo neurite orientation dispersion and density imaging of the human brain. *Neuroimage.* 61:1000–1016. https://doi.org/10.1016/j.neuroimage.2012.03.072.

Zhao B et al. 2021a. Common genetic variation influencing human white matter microstructure. *Science.* 372:eabf3736. https://doi.org/10.1126/science.abf3736.

Zhao B et al. 2021b. Large-scale GWAS reveals genetic architecture of brain white matter microstructure and genetic overlap with cognitive and mental health traits (n = 17,706). *Mol Psychiatry.* 26:3943–3955. https://doi.org/10.1038/s41380-019-0569-z.

Zou H, Hastie T. 2005. Regularization and variable selection via the elastic net. *J R Stat Soc Series B Stat Methodol.* 67:301–320. https://doi.org/10.1111/j.1467-9868.2005.00503.x.

Cerebral Cortex, 2025, **35**, bhaf199
https://doi.org/10.1093/cercor/bhaf199
Original Article